Journal Title
XX(X):1–20

DOI: 10.1177/ToBeAssigned
www.sagepub.com/
SAGE

Haptic Rendering and Interactive Simulation using Passive Midpoint Integration

Myungsin Kim, Yongjun Lee, Yongseok Lee and Dongjun Lee

Abstract

We propose a novel framework of haptic rendering and interactive simulation, which, exploiting the midpoint time integration, that is known for its superior energy-conserving property, yet, has not been adopted for haptics and interactive simulation, can enforce discrete-time passivity of the simulation effectively in practice while retaining real-time interactivity from its being non-iterative. We derive this PMI (passive midpoint integration) simulation for mechanical systems both in maximal coordinates (i.e., in SE(3)) and also in generalized coordinates (i.e., in $\Re^n$), with some potential actions as well to implement joint articulation, constraints, compliance, etc,; and also fully incorporate multi-point Coulomb frictional contact into them via PMI-LCP (linear complementarity problem) formulation. The proposed PMI-based simulation framework is applied to some illustrative examples to manifest its advantages: 1) haptic rendering of peg-in-hole task, where very light/stiff articulated objects can be simulated with multi-point contact; 2) haptic interaction with flexible beam, where marginally-stable/lossless behavior (i.e., vibration) can be stably emulated; and 3) under-actuated tendon-driven hand grasping, where mixed maximal-generalized coordinates are used with very light/stiff fingers.

Keywords

Haptic rendering, interactive simulation, linear complementarity problem, midpoint integration, passivity

1. Introduction

With many research groups and companies around the world aiming their effort to blur the boundary between the real world and virtual worlds in the form of, e.g., VR (virtual reality), AR (augmented reality), MR (mixed reality), etc., it is now increasingly in demand to provide realistic and believable artificial visual, auditory, olfactory, and mechanical experiences to users in real-time. Among these modalities, the artificial mechanical experience, or, haptic experience, possesses its own peculiar challenges, that is, as compared to other virtual sensory modalities, it requires much faster update rate while being under more stringent requirement for stability within the virtual world or with the human users.

Numerous strong results and methodologies have been proposed for realizing this virtual mechanical experience across different research communities. On one hand, in the field of haptics, it is pursued under the name of *haptic rendering*, for which some avatar of the haptic device (e.g., god-object (Zilles and Salisbury (1995)), virtual proxy (Colgate et al. (1995); Lee et al. (2012))) and the virtual objects are simulated together, typically under rather fast speed (e.g., 500Hz-1kHz), with their complexity encompassing from the simplest one-dimensional virtual wall (e.g., Colgate and Schenkel (1997); Lee and Huang (2008)) to complex deformable objects such as human organs (e.g., Delingette (1998); Duriez et al. (2006); Garre and Otaduy (2010)). On the other hand, in the field of computer animation (Baraff (1996); Müller et al. (2005); Weinstein et al. (2006); Garre et al. (2011)), it is often called by the name of *interactive simulation*, which typically deals with virtual objects and entities more complex than that of haptic rendering with slower update rate (e.g., 10-50Hz), which is yet fast enough for users to real-time interact. By utilizing multi-rate interface (e.g., Duriez et al. (2006); Fotoohi et al. (2007); Lee and Huang (2010)), it is also possible to combine the interactive simulation with haptic rendering.

The core of any frameworks in haptic rendering and interactive simulation of dynamical systems* is the time integration, and the majority of state-of-the-art frameworks adopts symplectic Euler integration (SEI (Hairer et al. 2006), also often referred to as semi-implicit Euler in the field of haptics and computer animation: e.g., Cline and Pai (2003); Müller et al. (2005); Weinstein et al. (2006)) or implicit Euler integration (IEI: e.g., Duriez et al. (2006); Otaduy and Lin (2006); Otaduy et al. (2009); Courtecuisse et al. (2015)). Widely-used commercial physics engines and interactive simulation tools also rely on the SEI (e.g., CHAI-3D (CHAI-3D 2004) based on ODE (ODE 2001), VREP (VREP 2010) based on ODE or Bullet (Bullet 2007)). The implicit Euler integration, in its exact form, is known to be (strictly) stable (e.g., Chung and Hulbert (1993); Hairer et al. (2006)),

The authors are with the Department of Mechanical & Aerospace Engineering and IAMD, Seoul National University, Seoul, 151-744, Korea

Corresponding author:
Dongjun Lee, Department of Mechanical & Aerospace Engineering and IAMD, Seoul National University, Seoul, 151-744, Korea.
Email: djlee@snu.ac.kr

*In contrast to quasi-static systems, for which time integration is typically not necessary (e.g., Ortega et al. (2007); Barbič and James (2008); Bender et al. (2013))

allowing for wide range of parameters (e.g., lighter mass with stiffer spring for transparency) and longer integration interval (i.e., faster simulation), yet, typically implemented only approximately for interactively-fast running (e.g., linearization (Duriez et al. (2006); Otaduy and Lin (2006)), explicitization (Krysl (2005, 2006))). This IEI is also in general strictly dissipative, thus, cannot simulate lossless or energy-conserving behaviors (e.g., vibrating flexible object). The symplectic Euler integration is usually simpler to implement (thus, faster) than the IEI due to its semi-implicit nature. This SEI, however, is known to be only conditionally stable (e.g., Hairer et al. (2006)), which turns out to be fairly detrimental in practice, as one cannot freely tune and explore parameters of virtual objects to achieve (possibly changing) target performance independently from other parts of the virtual world.

On the other hand, passivity has been one of the most powerful tools in the field of haptics, telerobotics and interactive robotics to enforce stability among dynamic entities coupled via feedback interconnection between, e.g., robots and humans, robots and robots, robots and environment (Colgate and Schenkel (1997); Lee and Huang (2010); Lee and Li (2005); Lee and Spong (2006); Buerger and Hogan (2007)). This passivity is particularly desirable for haptic rendering and interactive simulation, since, as pointed out in Brown and Colgate (1998), it would allow for: 1) stable simulation with *any* parameters and update-rate (e.g., arbitrarily light/stiff simulation with coarse integration interval); and 2) *modular* construction of provably-stable virtual world by simply combining individual virtual objects, each designed to be passive. Information delays among virtual objects or virtual worlds can also be addressed in a straightforward manner using this passivity formalism (e.g., for multi-user haptics Huang and Lee (2013); Rakhsha and Constantinescu (2014)).

In this paper, we propose a novel passivity-based framework of haptic rendering and interactive simulation. The key differentiating and innovative aspect of our framework is our adoption of the midpoint time integration, whose ability of energy-conserving is well-known in the field of structural mechanics (e.g., Chung and Hulbert (1993); Krysl (2006, 2005); Simo and Wong (1991); Simo et al. (1992); Kuhl and Crisfield (1999); Bathe (2007)), yet, to our knowledge, has not been adopted so far for haptic rendering and interactive simulation. This missing of the midpoint integration is particularly surprising for haptic rendering, as its energy-conserving property naturally suggests a possibility of discrete-time (lossless) passive simulation, that was proposed as one of the ultimate goals of haptic rendering in Brown and Colgate (1998, 1997), yet, has been dodging so far from any attempts to attain that. Of course, this energy-conserving property is only for a single system, and the passivity property, which concerns with their interconnection with other objects via power-conjugate input-output mapping, has not been studied in the structural mechanics field. It was however independently shown in (Lee and Huang (2008); Lee et al. (2012)) that, by directly enforcing passivity in the discrete-time domain similarly for the derivation of variational integrators (e.g., Marsden and West (2001)), it is indeed possible to develop a passive integrator, which is called NPMI (non-iterative passive mechanical integrator) and turns out to be a midpoint integrator. This NPMI derived in Lee and Huang (2008); Lee et al. (2012), however, is limited only to mechanical systems, that are linear or written in generalized coordinates with no intermittent and unilateral contact with other objects. Recently, we extended this NPMI for mechanical systems in maximal coordinates with LCP (linear complementarity problem) formulation of Coulomb friction contact (Kim et al. (2017)).

In this paper, we unify and generalize these NPMI-related results of Lee and Huang (2008); Lee et al. (2012); Kim et al. (2017) as a midpoint integration framework, that can deal with linear and nonlinear mechanical systems expressed both in generalized and maximal coordinates under unilateral/intermittent multi-point Coulomb friction contacts formulated via LCP, all the while effectively enforcing discrete-time passivity of the simulation and also its real-time interactivity by preserving the non-iterative nature of the NPMI. Some approximations, inevitable to render the algorithms interactively-fast, are also adopted here as for the most other haptic rendering and interactive simulation results (e.g., Duriez et al. (2006); Müller et al. (2005); Weinstein et al. (2006); Cline and Pai (2003); Otaduy and Lin (2006); Otaduy et al. (2009); Courtecuisse et al. (2015); Krysl (2005, 2006)). Even so, our proposed algorithms can still exhibit fairly passive behaviors, as manifested by our validating simulation examples (see Sec. 5) and also as similarly concluded in (Krysl (2005, 2006)) for midpoint integration with some approximations. Due to this reason, we call our integrator **passive midpoint integrator (PMI)** and our framework the PMI-based haptic rendering and interactive simulation.

Due to its passivity enforcement and implementation flexibility, our proposed PMI-based framework possesses the following advantages: 1) It can stably simulate mechanical objects with wide-range of parameters (e.g., any positive-definite mass, stiffness, and damping gains, and varying update-rate possible), thereby, allowing for easy and modular tuning of virtual objects while also providing capacity to adjust the discrete-time damping dissipation to render the simulation more or less stable depending on the target performance and behavior; 2) Consequently, it can simulate very light/stiff objects, which is desired for sharper/transparent haptic rendering (see peg-in-hole simulation of Sec. 5.1) or necessary to simulate some classes of mechanical systems (e.g., under-actuated tendon-driven (UATD) hand with light fingers and stiff tendons - see Sec. 5.3), yet, typically cannot be stably rendered by (conditionally-stable) SEI-based frameworks (e.g., CHAI-3D); 3) It can simulate marginally-stable/energy-conserving behaviors such as vibration of flexible objects (see Sec. 5.2 and also Sec. 2.3) or elastic contact between two rigid objects with no extra restitution models (see Sec. 3.3), that typically cannot be achieved by dissipative/decaying IEI-based frameworks, with its implementation complexity at least comparable to that of IEI; and 4) It allows us to use both the maximal and generalized coordinates and even their combination, substantially streamlining the simulation of some mechanical systems such as the UATD hand composed of fingers with tendon routing and rigid body plam (see Sec. 5.3) or the flexible beam with a rigid plate connected to

haptic devices (see Sec. 5.2), which is so far not so readily integrated in CHAI-3D or VREP. To our knowledge, this paper provides a solution for the first time to the long-standing problem posed in Brown and Colgate (1998, 1997), i.e., how to attain passivity and interactivity of simulation at the same time.

The rest of the paper is organized as follows. Sec. 2 contains some preliminary materials, including the definition of passivity, the kinematics and dynamics of rigid bodies in SE(3) and robots, and a summary of NPMI development for linear mechanical system in Lee and Huang (2008). We then derive the PMI-based simulation framework in maximal coordinates in Sec. 3 and in the generalized coordinates in Sec. 4 with the PMI-LCP formulation of Coulomb friction point contact modeling for each setting. Illustrative examples, namely, peg-in-hole task, flexible beam haptic interaction and UATD hand grasping, are presented in Sec. 5 to validate/demonstrate our PMI-based framework. Summary and some comments on the future research directions are then given in Sec. 6.

2. Preliminary

2.1. Mechanical Systems and Passivity

The virtual worlds, we aim to construct in this paper, are mainly composed of multiple articulated rigid bodies (Weinstein et al. (2006)) with some constraints (e.g., no penetration, rotation/pivot joints, etc.), elastic elements (e.g., springs), viscous damping elements, and Coulomb friction among them. A part of these mechanical objects is typically interfaced with some human commanding device (e.g., haptic device), the issue of which is not to be discussed here in detail and, instead, we refer readers to the prior results on the (possibly multi-rate) virtual coupling applicable to our PMI simulation (e.g., Lee and Huang (2010); Huang and Lee (2011); Lee et al. (2012)) and also to Sec. 5 for some application examples. Large-scale deformable objects (e.g., human organs Delingette (1998)) are not the main concern of this paper either and we leave them and their salient issues (e.g., model reduction, fast contact resolution, large deformation, St. Venant tensor simulation, etc.) for future publications, although the PMI framework is equally applicable for them as well (e.g., Huang and Lee (2013)).

Then, there are two ways to describe such articulated multiple rigid bodies: 1) *maximal coordinate*, which is the SE(3) rigid body transformation of each rigid body with the relative motion constraints implemented by Lagrange multipliers or some other means (e.g., Weinstein et al. (2006); Hadap (2006)); and 2) *generalized coordinate*, which is obtained by reducing the degree-of-freedom (DOF) of the total system directly applying their relative motion constraints (e.g., Lee et al. (2012); Spong et al. (2006)). The maximal coordinate approach is typically preferred for simulating complex systems (e.g., composed of large number of rigid bodies with possible collisions among them), whereas the generalized coordinate approach is more convenient or imperative for some mechanical systems (e.g., flexible beam with nodal coordinates, rigid links with elastic tendon routing, etc). Our rendering framework proposed in this paper allows for both of these maximal and generalized coordinates as well as their combination (see Sec. 5.2 and Sec. 5.3).

More specifically, the maximal coordinate approach simulates the articulated multiple rigid bodies as a combination of their constituent single rigid body, whose dynamics in SE(3) can be written by the following Newton-Euler dynamics s.t.,

$$m\ddot{x} + b_x\dot{x} + d\psi_x^T + \lambda_x = f + f_c \qquad (1)$$

$$J\dot{\omega} + \omega \times J\omega + b_w\omega + d\psi_w^T + \lambda_w = \tau + \tau_c \qquad (2)$$

$$\dot{R} = RS(\omega) \qquad (3)$$

where $x \in$ E(3) is the position with the mass $m > 0$, $b_x \in \Re^{3\times3}$ is positive semi-definite damping matrix, and $f \in \Re^3$ is to embed the exogenous force (e.g., virtual coupling), all expressed in the inertial frame $\{O\}$; whereas $R \in$ SO(3) is the rotation matrix of the body frame $\{B\}$ w.r.t. $\{O\}$, $\omega \in$ so(3) is the angular velocity, $J \in \Re^{3\times3}$ is the (constant) moment of inertia, $b_w \in \Re^{3\times3}$ positive semi-definite damping matrix, τ to embed the exogenous torque, all expressed in body frame $\{B\}$. Here, $\lambda_x, \lambda_w \in \Re^3$ are to be used to render the constraints among the rigid bodies to realize their articulation, for which we utilize potential-based approach (see Sec. 3.2); $f_c, \tau_c \in \Re^3$ are the contact force s.t., $f_c^T \cdot \dot{x} + \tau_c^T \cdot w \leq 0$ (e.g., with Coulomb friction - see Sec. 3.3); $d\psi_x, d\psi_w \in \Re^{1\times3}$ are the one-form of certain potential energy $\psi(x, R)$ s.t., $d\psi(x, R)/dt = d\psi_x \cdot \dot{x} + d\psi_w \cdot w$ (e.g., gravity or spring force - see Sec. 3.1); and $S(\star)$ is the skew-symmetric operator with $S(a)b = a \times b$, $a, b \in \Re^3$.

On the other hand, the dynamics of articulated rigid bodies in generalized coordinates can be written by the following continuous-time nonlinear Lagrangian dynamics s.t.,

$$M(q)\ddot{q} + C(q, \dot{q})\dot{q} + B\dot{q} + d\psi^T(q) = f + f_c \qquad (4)$$

where $q \in \Re^n$ is the configuration (i.e., generalized coordinates), $M(q) \in \Re^{n\times n}$ is the symmetric positive-definite inertia matrix, $C(q, \dot{q}) \in \Re^{n\times n}$ is the Coriolis matrix, $B \in \Re^{n\times n}$ is positive semi-definite damping matrix, $d\psi(q) \in \Re^{1\times n}$ is the one-form of potential energy function $\psi(q) \in \Re$ (e.g., gravity, spring potential) with $d\varphi/dt = d\varphi \cdot \dot{q}$, $f_c \in \Re^n$ is the contact force with $f_c^T\dot{q} \leq 0$ (e.g., with Coulomb friction), and $f \in \Re^n$ is to embed exogenous force (e.g., virtual coupling with haptic device).

It is then well-known that the mechanical system, represented in maximal coordinates (1)-(3) or in generalized coordinates (4) satisfies the (continuous-time) passivity (Spong et al. (2006)):

$$\int_0^T u^T y dt \geq E(T) - E(0), \quad \forall T \geq 0 \qquad (5)$$

with $E(t) := \kappa(t) + \psi(t)$ being the total energy, where $(u, y, \kappa) = ([f; \tau], [\dot{x}; w], (1/2)m\dot{x}^T\dot{x} + (1/2)w^T Jw)$ or $(u, y, \kappa) = (f, \dot{q}, (1/2)\dot{q}^T M(q)\dot{q})$ for the maximal coordinate formulation (1)-(3) or the generalized coordinate formulation (4), respectively. This passivity property (5) has been the key enabler of numerous nonlinear control techniques for mechanical systems, particularly those exploiting their nonlinear dynamics (1)-(3) or (4) (i.e., passivity-based control Spong et al. (2006); Slotine and Li (1987); Lee (2010); Lee and Lui (2017)) instead of

unnecessarily attempting to fully eliminate that (e.g., feedback linearization).

Further, from the passivity theorem (Vidyasagar (1993)) that feedback interconnection of *any* passive systems is necessarily stable regardless of their parameters (with some detectability condition met), this passivity property has been arguably the most powerful tool in telerobotics and haptics to ensure human-in-the-loop stability (e.g., Colgate and Schenkel (1997); Lee and Spong (2006); Huang and Lee (2013)). This also implies that, if we can simulate each virtual entity to be passive, we may then construct very a complex virtual world simply by combining those passive virtual entities, each of which can be designed individually without referring to other components and whose parameters can be set arbitrarily as long as passivity is preserved (e.g., any positive-definite M, B, K for (4), if $M(q) = M$ and $d\psi^T = Kq$ - see Sec. 2.2)l while also theoretically ensuring the stability of the whole virtual world. The benefits of passive simulation, namely, modular design, parameter-invariant stability, and theoretical stability guarantee, were recognized in Brown and Colgate (1998, 1997) and suggested as one of the ultimate goals of haptic rendering and interactive simulation.

This (fundamental) continuous-time passivity (5), yet, is in general not easily achievable in the discrete-time domain, particularly when the simulation speed needs to be haptically-fast. In fact, the work of Brown and Colgate (1998) shows that there does not exist any explicit discrete-time passive integrators. To address this, in Lee and Huang (2008), we proposed a new integrator, non-iterative passive mechanical integrator (NPMI), which is implicit, yet, requires no iterations, thus, can still be solved haptically-fast while also enforcing discrete-time passivity. This NPMI turns out to be a midpoint integrator, and is to be generalized in this paper to be PMI (passive midpoint integrator). In the next Sec. 2.2, we summarize the result of Lee and Huang (2008), which stands as the backbone of the ensuing development of PMI-based haptic rendering and interactive simulation framework of this paper.

2.2. Review of NPMI for Linear Mechanical Systems

To introduce the main idea of NPMI (Lee and Huang (2008)), let us consider the following simple scalar linear mass-damper-spring dynamics:

$$ma + bv + kx = f$$

where $x \in \Re$, $v = \dot{x} \in \Re$, $a = \ddot{x} \in \Re$ are the position, velocity and acceleration, $m, b, k > 0$ are the mass, damper and spring coefficients, and $f \in \Re$ is the exogenous force, respectively. The passivity property (5) is then given by: during $T_k = [t_k, t_{k+1})$,

$$\int_{t_k}^{t_{k+1}} fvdt = \frac{1}{2}m(v_{k+1}^2 - v_k^2) + \frac{1}{2}k(x_{k+1}^2 - x_k^2) + \int_{t_k}^{t_{k+1}} bv^2 dt$$

where $\star_k := \star(t_k)$. Let us denote by $\hat{\star}_k$ to be "representative" $\star_k$ for the duration T_k. Then, we can approximate the above passivity relation s.t.,

$$\begin{aligned}\hat{f}_k\hat{v}_kT_k &= \frac{1}{2}mv_{k+1}^2 - \frac{1}{2}mv_k^2 + \frac{1}{2}kx_{k+1}^2 - \frac{1}{2}kx_k^2 + b\hat{v}_k^2T_k \\ &= \frac{1}{2}(v_{k+1} - v_k)m(v_{k+1} + v_k) \\ &\quad + \frac{1}{2}(x_{k+1} - x_k)k(x_{k+1} + x_k) + b\hat{v}_k^2T_k \end{aligned} \tag{6}$$

where we also use $T_k := t_{k+1} - t_k$ with a slight abuse of notation.

Our goal here is then to find a discrete-time integrator map

$$\mathcal{L} : (x_k, v_k, f_k) \to (x_{k+1}, v_{k+1})$$

and the representative power variables $\hat{v}_k, \hat{f}_k$ so that the map $\mathcal{L}$ exactly duplicates the continuous-time passivity relation (6), or, equivalently, its differential form

$$f^T v = v(ma + bv + kx) \tag{7}$$

By comparing (6) with (7), the NPMI then suggests the following kinematics relation (Lee and Huang (2008)):

$$\hat{v}_k := \frac{v_{k+1} + v_k}{2} = \frac{x_{k+1} - x_k}{T_k} \tag{8}$$

and, further, applying (8) to (6) and comparing that with (7), it also suggests the following dynamics update equation:

$$m\frac{v_{k+1} - v_k}{T_k} + b\hat{v}_k + k\hat{x}_k = f_k \tag{9}$$

with $\hat{x}_k := \frac{x_{k+1}+x_k}{2}$ and $\hat{f}_k = f_k$.

This NPMI (8)-(9) then exactly duplicates the continuous-time passivity property (5) by using the "representative" velocity $\hat{v}_k$ and position $\hat{x}_k$. For the choice of $\hat{f}_k$, we have latitude, thus, we choose $\hat{f}_k = f_k$ for simplicity of the integrator $\mathcal{L}$. With these "representative" quantities, the NPMI then satisfies the following discrete-time passivity:

$$\begin{aligned}\sum_{k=0}^{N-1} f_k\hat{v}_kT_k &= \frac{1}{2}m(v_N^2 - v_o^2) + \frac{1}{2}k(x_N^2 - x_o^2) + \sum_{k=0}^{N-1} b\hat{v}_k^2T_k \\ &\geq -\frac{1}{2}mv_o^2 - \frac{1}{2}kx_o^2 = -E_o \end{aligned} \tag{10}$$

$\forall N \geq 0$, i.e., the maximum extractable energy from the system is lower bounded by the system initial energy. Since it is derived directly by enforcing certain physical principle (i.e., passivity) in the discrete-time domain, the NPMI is a geometric integrator similar to variational integrators (e.g., Marsden and West (2001)), which discretizes the variational principle itself.

This NPMI (8)-(9) also turns out to be a midpoint integrator (e.g., Krysl (2006, 2005); Simo et al. (1992); Kuhl and Crisfield (1999); Bathe (2007)), which is well-known for its superior energy-conserving property (i.e., passivity, yet, with no input-output consideration) in structural mechanics community, yet, has not been adopted so far for haptic rendering and interactive simulation. In this paper, we generalize this NPMI as passive midpoint integrator (PMI), with full consideration of input-output mapping (i.e., power port), generalized and maximal coordinate formalisms, nonlinear dynamics (1)-(4), and constraints and

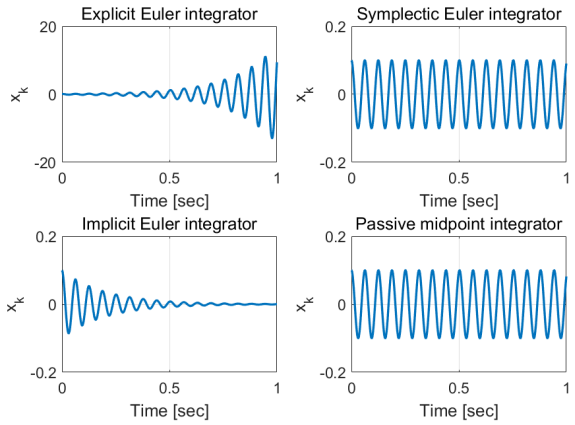

Figure 1. Simple harmonic oscillation simulation with EEI, SEI, IEI and PMI: $m = 0.01$[kg], $k = 100$[N/m], $T_k = 0.001$[sec].

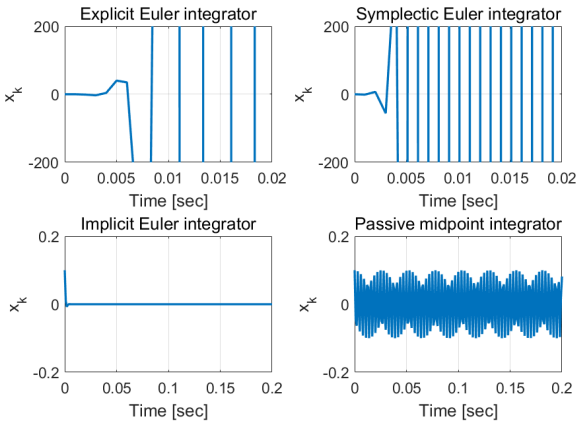

Figure 2. Simple harmonic oscillation simulation with EEI, SEI, IEI and PMI: $m = 0.00001$[kg], $k = 100$[N/m], $T_k = 0.001$[sec].

multi-point contacts with Coulomb friction, all the while retaining its discrete-time passivity and non-iterativeness by utilizing certain coordinate transformation and potential action approximation.

Of course, other types of integrators have also been used for haptic rendering and interactive simulation, namely, explicit Euler integrator (EEI), symplectic Euler integrator (SEI) and implicit Euler integrator (IEI), with the second being adopted for the majority of widely-used open physics engines (e.g., Bullet and ODE, with VREP and CHAI-3D built upon them). In the next Sec. 2.3, we perform a simple, yet, effective comparison study among these EEI, SEI, IEI and PMI.

2.3. Comparison of EEI, SEI, IEI and PMI

Consider the simple scalar linear mass-spring system, which can be written by

$$
\begin{aligned}
m\frac{v_{k+1}-v_k}{T_k} + kx_k &= f_k \qquad & x_{k+1} &= x_k + v_k T_k \\
m\frac{v_{k+1}-v_k}{T_k} + kx_k &= f_k \qquad & x_{k+1} &= x_k + v_{k+1} T_k \\
m\frac{v_{k+1}-v_k}{T_k} + kx_{k+1} &= f_k \qquad & x_{k+1} &= x_k + v_{k+1} T_k \\
m\frac{v_{k+1}-v_k}{T_k} + k\hat{x}_k &= f_k \qquad & x_{k+1} &= x_k + \hat{v}_k T_k
\end{aligned}
$$

presented in the order of EEI, SEI, IEI and PMI, where $\hat{x}_k, \hat{v}_k$ are defined in (8)-(9). Note the difference in their rendering spring force: kx_k (EEI and SEI), kx_{k+1} (IEI), and $k\hat{x}_k$ (PMI). Note also that each integrator adopts different "representative" velocity: v_k (EEI), v_{k+1} (SEI and IEI), and $\hat{v}_k$ (PMI).

Then, adopting the procedure similar to that in Sec. 2.2, we can obtain the passivity property of each integrator as follows. First, for the EEI, we have

$$
\sum_{k=0}^{N-1} f_k v_k T_k \leq \frac{1}{2} m(v_N^2 - v_0^2) + \frac{1}{2} k(x_N^2 - x_0^2)
$$

for which we utilize

$$
\begin{aligned}
\sum_{k=1}^{N} m\frac{v_{k+1}-v_k}{T_k} v_k T_k &\leq \frac{1}{2} m v_{N+1}^2 - \frac{1}{2} m v_0^2 \\
\sum_{k=1}^{N} k x_k \frac{x_{k+1}-x_k}{T_k} T_k &\leq \frac{1}{2} k x_{N+1}^2 - \frac{1}{2} k x_0^2
\end{aligned} \qquad (11)
$$

derived by using Cauchy-Schwarz inequality. This then implies that EEI is in general not passive. Similarly, for the IEI, we have

$$
\sum_{k=0}^{N-1} f_k v_{k+1} T_k \geq \frac{1}{2} m(v_N^2 - v_0^2) + \frac{1}{2} k(x_N^2 - x_0^2)
$$

for which we utilize

$$
\begin{aligned}
\sum_{k=1}^{N} m\frac{v_{k+1}-v_k}{T_k} v_{k+1} T_k &\geq \frac{1}{2} m v_{N+1}^2 - \frac{1}{2} m v_0^2 \\
\sum_{k=1}^{N} k x_{k+1} \frac{x_{k+1}-x_k}{T_k} T_k &\geq \frac{1}{2} k x_{N+1}^2 - \frac{1}{2} k x_0^2
\end{aligned} \qquad (12)
$$

This then implies that IEI is passive, yet, in general dissipative, thus, not able to simulate such lossless behaviors as harmonic oscillation. On the other hand, for the SEI, its passivity is undetermined, since its relation is a combination of (12) (i.e., passive) with (11) (i.e., non-passive). This in fact well matches with the known fact that the SEI is only conditionally stable depending on parameters. Finally, for the PMI, we have

$$
\sum_{k=0}^{N-1} f_k \hat{v}_k T_k = \frac{1}{2} m(v_N^2 - v_0^2) + \frac{1}{2} k(x_N^2 - x_0^2)
$$

from (10), implying that it is passive, and, further, exactly lossless, thus, can precisely simulate harmonic oscillation.

This observation is then confirmed by the simulation results in Fig. 1 and Fig. 2, where: 1) the EEI always diverges; 2) the SEI can simulate harmonic oscillation with large mass, yet, diverges with small mass; 3) the IEI always converges to zero, yet, not able to sustain harmonic oscillation, clearly showing its dissipativeness; and 4) only

the PMI can simulate harmonic oscillation with the total energy exactly conserved for any mass/spring ratio. This then clearly shows the advantage of our PMI, namely, its ability to passive (i.e., stable) simulation with wide-range of parameters as compared to EEI and SEI, while also being typically simpler to implement than IEI on top of its ability to simulate lossless behaviors.

3. PMI-Based Simulation in Maximal Coordinates

The NPMI (8)-(9) of Sec. 2.2 exactly enforces passivity only for linear mechanical systems. Here, we generalize this NPMI to passive midpoint integration (PMI) of rigid bodies in SE(3), which constitute the basic building block of the maximal coordinate formalism of articulated rigid bodies. We also show how to incorporate constraints into this PMI-based simulation of rigid bodies to realize articulation among the rigid bodies, and how to render multi-point Coulomb friction contact via LCP (linear complementarity problem) formulation into the framework of PMI. The main complication for this is that the configuration space of rigid bodies in maximal coordinate is SE(3), which is not a vector space. The multi-point contact computation problem is also typically complex and time-consuming. To circumvent these challenges, here, we utilize some approximations in enforcing passivity. Such approximation is in general necessary for other haptic rendering or interactive simulation results to attain interactivity (e.g., contact force linearization with IEI or SEI Otaduy and Lin (2006)) or for structural dynamics to speed up the computation (e.g., interaction explicitation Bathe (2007); Krysl (2005, 2006)), which yet is known to work adequately in most cases as also confirmed through our experiments as well (see Sec. 5)

3.1. PMI of Rigid Body in SE(3)

Consider the Newton-Euler dynamics (1)-(3) of rigid bodies in SE(3). In this Sec. 3.1, we derive the PMI formulation of (1)-(3). For this, we consider only the inertial dynamic (i.e., associated with m, J), the potential action (i.e., $d\psi_\star$), and the exogenous forcing f, τ. The constraint and contact forces (i.e., $\lambda_\star, f_c, \tau_c$) will be added in Sec. 3.2 and Sec. 3.3, respectively. We also restrict the potential ψ in this Sec. 3.1 to be the linear E(3) spring directly acting on x (i.e., $\psi = \psi_x = \frac{1}{2}x^T k_x x$) or the SO(3) spring acting on R (i.e., $\psi = \psi_w(R)$), while postponing the treatment of more general $\psi(x, R)$ to Sec. 3.2.

Then, with the linear spring potential $\psi_x = \frac{1}{2}x^T k_x x$, the translation dynamics (1) can simply be simulated via the linear NPMI (8)-(9) while exactly enforcing passivity as stated in Sec. 2.2. The attitude dynamics (2) also has the structure similar to that of linear NPMI (9) except the coupling term $w \times Jw$, which can be written by $w \times Jw = -S(Jw)w$, where $S(Jw) \in \Re^{3\times 3}$ is skew-symmetric with $a^T S(Jw)a = 0\ \forall a \in \Re^3$. This then suggests the following PMI expression of the attitude dynamics (2):

$$J\frac{\omega_{k+1} - \omega_k}{T_k} - S(J\omega_k)\hat{\omega}_k + b_w\hat{\omega}_k + d\psi_{w_k}^T = \tau_k \quad (13)$$

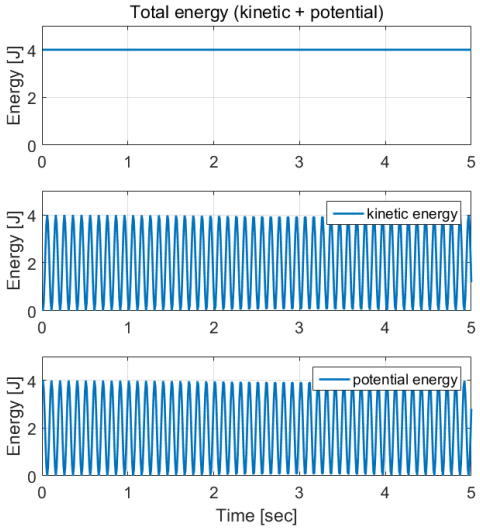

Figure 3. Total energy of rotational dynamics (13) with SO(3) spring (20) with nearly perfect energy conservation and stable/sustained oscillation in SO(3): with $J = 0.001 \cdot I$[kg m^2], $k_w = 1$ [Nm/rad] and $T_k = 0.01$ [sec] starting from $\phi_o = 0.9\pi$ along the direction of $\frac{1}{\sqrt{6}}(1, 2, 1)$.

with the "representative" angular velocity

$$\hat{w}_k := \frac{w_{k+1} + w_k}{2} \quad (14)$$

similar to (8). It is then not difficult to show the following passivity (lossless) property with $\psi_w = 0$ similar to (10):

$$\sum_{k=0}^{N-1} \tau_k^T \hat{\omega}_k T_k = \frac{1}{2}w_N^T J w_N - \frac{1}{2}w_o^T J w_o \geq -\frac{1}{2}w_o^T J w_o \quad (15)$$

where we use $\hat{w}_k^T S(Jw_k)\hat{w}_k = 0,\ \forall k = 0, ..., N-1$. The coupling term $S(Jw)w$ is often omitted in computer graphics literatures. For this case, the PMI expression (13) simply reduces to the linear NPMI (9).

One thing still missing here is how to connect the angular velocity $\hat{w}_k \in \Re^3$ in (14) to the rotation matrix $R_k \in$ SO(3) while ensuring passivity as much as permissible for interactivity requirement. For this, we utilize the following discrete-time version of the rotational kinematics (3) s.t.,

$$R_{k+1} = R_k \exp(S(\hat{\omega}_k T_k)) \quad (16)$$

where $\exp(\star)$ is the exponential map (Murray et al. (1993)). This discrete-time kinematics equation (16) in SO(3) then should be compatible with the SO(3) spring potential, as so are true for $\hat{v}_k, \hat{x}_k$ and $\psi_k = \frac{1}{2}kx_k^2$ in Sec. 2.2. For this, define the following SO(3) spring potential:

$$\psi_w := \frac{1}{2}k_w\phi^2(R, R_o) \quad (17)$$

with $k_w > 0$ and

$$\phi(R, R_o) := \|\log(R^T R_o)\| =: \cos^{-1}\gamma$$

where $R_o \in$ SO(3) is the reference rotation, $\mathrm{tr}(\star)$ and $\log(\star)$ are the trace and matrix logarithm operators, and

$$\gamma = \frac{1}{2}[\mathrm{tr}(R^T R_o) - 1]$$

This ϕ is known to be the geodesic on the unit sphere (Huynh (2009)). This SO(3) spring, of course, is practically important as well, e.g., directly applicable to implement virtual coupling between two large-rotation rigid bodies (e.g., virtual coupling for palm and fingers of multi-fingered hand - see Fig. 4).

Our objective is then to find the action $d\psi_{w_k}$ for (13) to implement the SO(3) spring (17) under the passivity requirement. For this, particularly due to that SO(3) is not a vector space differently from that for the linear NPMI (9), we attempt to enforce passivity only approximately, which, yet, turns out to work fairly well as shown below. More precisely, we aim to define $d\psi_{w_k}$ s.t.,

$$d\psi_{w_k}\hat{\omega}_k T_k = \frac{\partial \psi_w}{\partial \phi}\Delta\phi_k + \frac{1}{2}\frac{\partial^2 \psi_w}{\partial \phi^2}\Delta\phi_k^2 \qquad (18)$$

which is the second-order approximation of exact potential difference (i.e., $\psi_{w,k+1} - \psi_{w_k}$), with $\partial\psi_w/\partial\phi = k_w\phi_k$ and $\partial^2\psi_w/\partial\phi^2 = k_w$. For (18), we also use

$$\Delta\phi_k = \frac{\partial\phi}{\partial\gamma}\Delta\gamma_k, \quad \Delta\gamma_k := \frac{1}{2}\hat{\omega}_k^T\bar{\omega}_k T_k \qquad (19)$$

where $\partial\phi/\partial\gamma = -1/\sin\phi_k$ and $\bar{\omega}_k \in \Re^3$ is defined s.t.,

$$S(\bar{\omega}_k) := R_k^T R_o - R_o^T R_k$$

which has the direction of the equivalent axis between R_k and R_o and the magnitude $\|\bar{\omega}_k\| = 2\sin(\phi_k)$; and the term $\Delta\gamma_k$ is designed s.t.,

$$\begin{aligned}\Delta\gamma_k &= \frac{1}{2}\operatorname{tr}[R_{k+1}^T R_o - R_k^T R_o] \approx \frac{1}{2}\operatorname{tr}[S^T(\hat{\omega}_k T_k)R_k^T R_o] \\ &= \frac{1}{4}\operatorname{tr}[S^T(\hat{\omega}_k T_k)(R_k^T R_o - R_o^T R_k)]\end{aligned}$$

which is reduced to (19), where we use (16), the first order approximation of $\exp(S(\hat{w}_k T_k)) \approx I + S(\hat{w}_k T_k)$, and the properties of $\operatorname{tr}(\star)$, e.g., $\operatorname{tr}(A+B) = \operatorname{tr}(A) + \operatorname{tr}(B)$, $\operatorname{tr}(ABC) = \operatorname{tr}(BCA)$, $\operatorname{tr}(A) = \operatorname{tr}(A^T)$, and $a^T b = \operatorname{tr}[S^T(a)S(b)/2]$, $\forall a, b \in \Re^3$.

Applying these to (18), we can then define $d\psi_{w_k}$, s.t.,

$$d\psi_{w_k}^T = -\frac{k_w\phi_k}{2\sin\phi_k}\bar{\omega}_k + \frac{1}{8}\frac{k_w T_k}{\sin^2\phi_k}(\bar{\omega}_k\bar{\omega}_k^T)\hat{\omega}_k$$

where $\bar{\omega}_k\bar{\omega}_k^T \in \Re^{3\times 3}$ is a rank one matrix. Since $||\bar{\omega}_k|| = 2\sin(\phi_k)$, we can further approximately simplify $d\psi_{w_k}$ s.t.,

$$d\psi_{w_k}^T \approx -\frac{k_w\phi_k}{2\sin\phi_k}\bar{\omega}_k + \frac{k_w T_k}{2}\hat{\omega}_k \qquad (20)$$

where note that the second term acts similarly as viscous damping action. The passivity of this SO(3) spring action (20) is then demonstrated in Fig. 3, where stable sustained oscillation is attained with the total energy almost precisely preserved even if the action (20) is designed to enforce passivity only approximately.

Finally, the PMI expression of the Newton-Euler dynamics (1)-(2) with the linear spring for x and the SO(3) spring potential (20) can be written in one single equation:

$$M\frac{V_{k+1} - V_k}{T_k} + C_k(\omega_k)\hat{V}_k + B\hat{V}_k + d\psi_k^T = F_k$$

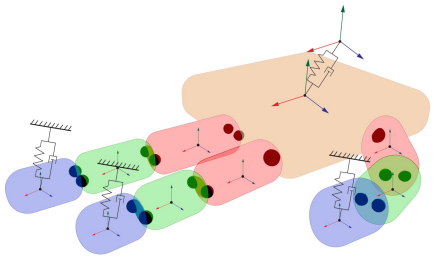

Figure 4. Multi-fingered hand rendered as articulated multiple rigid bodies with joints implemented by point constraint springs.

where $V_k := [v_k; \omega_k] \in \Re^6$ with $\hat{V}_k := [\hat{v}_k; \hat{\omega}_k] \in \Re^6$, $M := \operatorname{diag}[mI_{3\times 3}, J] \in \Re^{6\times 6}$ is the inertia matrix, $C_k := \operatorname{diag}[0_{3\times 3}, -S(J\omega_k)]$ with $C_k = -C_k^T$, $B := \operatorname{diag}[b_x, b_\omega] \in \Re^{6\times 6}$ is the damping matrix, $d\psi_k^T := [k_x\hat{x}_k; d\psi_{\omega_k}^T] \in \Re^6$ is the potential action as defined in (9) and (20), and $F_k := [f_k; \tau_k] \in \Re^6$ is the exogenous wrench. This equation can also be written in the following form, which is to be used for the ensuing developments:

$$\hat{M}_k\hat{V}_k = M_k V_k - d\bar{\psi}_k^T + F_k \qquad (21)$$

where $\hat{M}_k := [M_k + C_k + B + (T_k/2)K] \in \Re^{6\times 6}$ with $M_k := 2M/T_k$, $K := \operatorname{diag}[k_x, k_\omega] \in \Re^{6\times 6}$ is the spring matrix from (9) and (20), and $d\bar{\psi}_k^T := [-k_x x_k; \frac{k_\omega\phi_k}{2\sin\phi_k}\bar{\omega}_k] \in \Re^6$ from (20). Here, both $\hat{M}_k$ and M_k are non-singular.

3.2. PMI-Based Rendering of Articulated Rigid Bodies

One of the most widely used entities in haptic rendering and interactive simulation are so called articulated rigid bodies (e.g., Weinstein et al. (2006)). Here, we propose to construct such articulated rigid bodies as a collection of multiple rigid links with their joints implemented by constraining position of some points on the successive links via very stiff spring. For instance, see the multi-fingered hand in Fig. 4, where the DIP and MCP joints of the index finger are implemented by enforcing two-point position constraints on distal-middle and middle-proximal phalanxes; whereas the thumb CMC joint by one single-point position constraint between the palm and the metacarpal bone. Other types of joint constraints can also be implemented in a similar manner by using different spring potentials (e.g., elliptic joint with four-point springs (Knoop et al. 2005); prismatic joint with a SO(3)-potential and a two-directional translation spring potential, etc.), details of which will be reported in future publications.

Consider m rigid-links with l-point position constraints (e.g., $m = 10$ and $l = 16$ for the hand in Fig. 4). We assume each of these l-points be shared only by two successive links, although the development presented here can easily be extended to more general cases. Then, we can define the following map

$$c_1, c_2 : \{1, 2, ..., l\} \mapsto \{1, 2, ..., m\}$$

i.e., connecting the i-th position constraining point ($i \in \{1, 2, ..., l\}$) to its presence on the $c_1(i)$-th and the $c_2(i)$-th links. We can then denote this presence of the i-th

constraining-point by

$$p_{i,j} := x_{c_j(i)} + R_{c_j(i)} r_{c_j(i),i} \in \Re^3, \;\; j = 1, 2$$

which is on the $c_j(i)$-th link with the offset from $x_{c_j(i)}$ given by $r_{c_j(i),i} \in \Re^3$ expressed in the $c_j(i)$-th link body fixed frame.

To implement the joints among the m-link, we then want to enforce

$$\Delta p_i := p_{i,1} - p_{i,2} \equiv 0$$

Stacking up all the l-point position constraints, define the constraint function $G : \Re^{3l} \to \Re^{3l}$ s.t.,

$$G := [\Delta p_1; \Delta p_2; ...\Delta p_l]$$

with $G = 0$ implying that all the l-point position constraints are ensured, and so are the joints among the m-links. We can then first-order approximate this G s.t.,

$$G_{k+1} \approx G_k + J_k \hat{V}_k T_k \tag{22}$$

where $\hat{V}_k = [\hat{v}_{1_k}; \hat{\omega}_{1_k}; \hat{v}_{2_k}; \hat{\omega}_{2_k}; ...; \hat{v}_{m_k}; \hat{\omega}_{m_k}] \in \Re^{6m}$ contains the representative velocities of all the m rigid bodies, and $J \in \Re^{3l \times 6m}$ is the Jacobian defined s.t., $dG/dt = JV$.

The PMI expression of the dynamics of the m rigid links with the l-constraints can then be written similar to (21) s.t.,

$$\hat{M}_k \hat{V}_k = M_k V_k - d\bar{\psi}_k^T + J_k^T \lambda_k + F_k \tag{23}$$

where $\lambda_k \in \Re^{3l}$ is to embed certain potential action to robustly maintain the constraint $G = 0$ similar to the penalty-based contact formulation (Drumwright 2008; Hasegawa and Fujii 2003), and all the other terms are defined for the m rigid bodies similarly to those in (21). Our goal is then to design the potential action λ_k to attain the constraint $G = 0$ while also respecting the passivity requirement. For this, let us define the following potential function associated with the (target) constraint $G = 0$:

$$\psi_{\lambda_k} := \frac{1}{2} k_\lambda G_k^T G_k$$

where $k_\lambda > 0$ is a constant.

Then, using (10), (15), (18), (22) and (23), we can obtain

$$\begin{aligned} &F_k^T \hat{V}_k T_k \\ &\approx \kappa_{k+1} - \kappa_k + \psi_{k+1} - \psi_k + \hat{V}_k^T B \hat{V}_k T_k - \hat{V}_k^T J_k^T \lambda_k T_k \end{aligned}$$

where $\kappa_k := \frac{1}{2} V_k^T M V_k$ is the kinetic energy, M is the inertia matrix and $\psi_k = \frac{1}{2} x_k^T k_x x_k + \psi_{w,k}$ of the m rigid bodies collective as defined before (21). Further, utilizing the second-order approximation of

$$\psi_{\lambda_{k+1}} - \psi_{\lambda_k} \approx k_\lambda G_k^T J_k \hat{V}_k T_k + \frac{1}{2} k_\lambda \hat{V}_k^T J_k^T J_k \hat{V}_k T_k^2 \tag{24}$$

we can design

$$\lambda_k = -k_\lambda [G_k + \frac{1}{2} J_k \hat{V}_k T_k] \tag{25}$$

with which the above relation reduces to: with $B = 0$,

$$F_k^T \hat{V}_k T_k \approx E_{k+1} - E_k$$

where $E_k := \frac{1}{2} V_k^T M V_k + \psi_k + \psi_{\lambda,k}$ is the total energy. With this λ_k of (25), (23) can also be written by

$$\left[\hat{M}_k + \frac{k_\lambda T_k}{2} J_k^T J_k\right] \hat{V}_k = M_k V_k - k_\lambda J_k^T G_k - d\bar{\psi}_k^T + F_k \tag{26}$$

The analysis above shows that the potential action λ_k (25) would robustly enforce the constraint $G = 0$ while also nearly enforcing the passivity of the PMI simulation of articulated rigid bodies. Here, note that the passivity is enforced only approximately, as we adopt the potential action approximation (24), which in turn stems from our adoption of the Jacobian approximation (22). We have this nonlinear potential approximation (24) even if the potential ψ_{λ_k} itself is only quadratic, since the maximal coordinates are on a non-vector space SE(3). This potential action approximation (24) is crucial to render the PMI simulation still non-iterative even with the nonlinear potential ψ_{λ_k}. The "lack" of passivity due to this potential action approximation (24) can also be easily amended by injecting (typically) small amount of damping B, which can also be incorporated into the PMI simulation while retaining its non-iterative structure (26).

This passive constraint-enforcing $G = 0$ turns out to be very useful, since it allows us to utilize very large stiffness (i.e., k_λ) to enforce the joint articulations, even for very light rigid links (e.g., to render light virtual proxy for transparency) - see Sec. 5.1. Note that we can also implement the spring potential action $\psi(x, R)$ (e.g., spring connected not on the center-of-mass x of rigid bodies) by using the same procedure to design λ_k proposed here, that is, define the spring connection point positions similar to G, define their spring potentials similar to ψ_λ, and design the potential action $d\psi$ similar to λ_k to respect the approximated potential difference equation. Here, we also adopt this "soft" potential action ψ_{λ_k} to enforce the constraint $G = 0$ instead of the "hard" Lagrange multiplier approach for (22), since: 1) the latter is much less robust (e.g., drift) with the Jacobian approximation (22) than the former, which contains potential action similar to the penalty-based contact formulation (Drumwright 2008; Hasegawa and Fujii 2003); and 2) the passivity of the former is easily achievable (with small damping B injection), whereas that of the latter still unclear.

3.3. PMI-LCP for Multi-Point Coulomb Friction Contact

The contact problem has been one of the key problems in computer graphics, structural mechanics and haptic rendering. For this, there are two main directions of research, namely, constraint based method (e.g., Duriez et al. (2006); Peterlik et al. (2011)) and penalty based method (e.g., Kolesnikov and Zefran (2007); Drumwright (2008)). The penalty based method generates repulsive elastic force when two objects overlap with each other. This method is simple and easy to implement, yet, it has its inherent limitation, i.e., allowing violation of the contact constraint (e.g., penetration). It is in general not straightforward either to implement Coulomb friction force with this penalty based method. On the other hand, the constraint based method directly calculates contact force, that is necessary to satisfy the contact constraint. By doing so, this method prevents the

violation of the constraint (to the extent of collision detection error and numerical precision error though, which can induce constraint drift). Friction generation is also more convenient with the constraint based method.

To render the contact among rigid objects, we adopt the point contact model with Coulomb friction. Consider a contact point between two colliding rigid bodies. We can then define the contact normal direction $\vec{n}(t) \in \Re^3$ and the penetration depth along that direction. Denote this depth by $d(t) \geq 0$, with $d(t) = 0$ and $d(t) > 0$ respectively implying contact and no contact. Whenever $d(t) = 0$ occurs, the following higher-order conditions can be utilized to enforce no penetration constraint:

$$\dot{d} \geq 0, \;\; \ddot{d} \geq 0, \;\; \cdots$$

with the non-negative signs allowing only for separation or keeping the contact. In this paper, we use the velocity-level constraint, which can then be written as the following complementarity condition (Siciliano and Khatib (2008)):

$$0 \leq \dot{d} \perp \lambda^n \geq 0 \tag{27}$$

where $\lambda^n \geq 0$ is the contact force along $\vec{n}$.

Now, suppose that the articulated rigid bodies (23) interact with another virtual rigid object, and denote the i-th contact point from that contact by

$$p_i^c := x_{c(i)} + r_i^c$$

which is on the $c(i)$-th link and occurs at the offset of $r_c^i \in \Re^3$ from its center-of-mass (expressed in the inertial frame), where $c : \{1, 2, ..., l_c\} \to \{1, 2, ..., m\}$ is the mapping from the contact points to their associated rigid link from the articulated rigid bodies (23). The contact wrench, which is to be embedded in F_k of (23) is then given by

$$F_{i,k}^c = \underbrace{\begin{bmatrix} I & -S(r_{i,k}^c)R_{\sigma(i),k} \end{bmatrix}}_{=:Ad_{i,k}^c \in \Re^{3\times 6}}{}^T f_{i,k}^c \in \Re^6 \tag{28}$$

where $Ad_{i,k}^c$ is the (partial) contact adjoint operator Murray et al. (1993). The contact force $f_{i,k}^c \in \Re^3$ is defined following the point contact and Coulomb friction model (Siciliano and Khatib (2008)) s.t.,

$$\begin{aligned} f_{i,k}^c &= \vec{n}_k \lambda_{i,k}^n + \left[\vec{t}_{i,k}^1, \vec{t}_{i,k}^2, \cdots, \vec{t}_{i,k}^{\bar{p}}\right] \left[\lambda_{i,k}^{t_1}; \lambda_{i,k}^{t_2}; \cdots; \lambda_{i,k}^{t_{\bar{p}}}\right] \\ &=: N_{i,k}\lambda_{i,k}^n + D_{i,k}\lambda_{i,k}^t \end{aligned} \tag{29}$$

where $\lambda_{i,k}^n \geq 0$ is the normal contact force, $\lambda_{i,k}^t \in \Re^{\bar{p}}$ is the tangential friction forces, for which we utilize the $\bar{p}$-sides pyramidal cone approximation Duriez et al. (2006), $\vec{n}_{i,k}, \vec{t}_{i,k}^j \in \Re^3$ are the normal and tangential direction vectors, and $N_{i,k} \in \Re^3, D_{i,k} \in \Re^{3\times\bar{p}}$ are the stacking matrix of $\vec{n}_{i,k}$ and $\vec{t}_{i,k}^j$.

The PMI expression of the articulated rigid bodies, the virtual object, and their contact interaction can then be obtained by augmenting (26) s.t.,

$$\begin{aligned} &\underbrace{\begin{bmatrix} \hat{M}_k + \frac{k_\lambda T_k}{2} J_k^T J_k & 0 \\ 0 & \hat{M}_k^o \end{bmatrix}}_{=:A_k \in \Re^{6(m+1)\times 6(m+1)}} \underbrace{\begin{pmatrix} \hat{V}_k \\ \hat{V}_k^o \end{pmatrix}}_{=:\hat{V}_k^a \in \Re^{6(m+1)}} \\ &= \underbrace{\begin{pmatrix} M_k V_k - k_\lambda J_k^T G_k - d\bar{\psi}_k^T \\ M_k^o V_k^o \end{pmatrix}}_{=:B_k \in \Re^{6(m+1)}} + F_k^c \end{aligned}$$

with the contact force term $F_k^c \in \Re^{6(m+1)}$ defined by

$$F_k^c := \bar{N}_k \lambda_k^n + \bar{D}_k \lambda_k^t$$

where $\lambda_k^n := [\lambda_{1,k}^n; \lambda_{2,k}^n; ...; \lambda_{l_c,k}^n] \in \Re^{l_c}$ and $\lambda_k^t := [\lambda_{1,k}^t; \lambda_{2,k}^t; ...; \lambda_{l_c,k}^t] \in \Re^{l_c\times\bar{p}}$ are the collection of the normal contact and tangential friction forces of all the l_c contact points, and the matrices $\bar{N}_k \in \Re^{6(m+1)\times l_c}$ and $\bar{D}_k \in \Re^{6(m+1)\times(l_c\times\bar{p})}$ are the matrices specifying the directions of λ_k^n and λ_k^t with $Ad_{i,k}^c$ in (28) embedded in them. We can then rewrite the above PMI simulation equation s.t.,

$$\hat{V}_k^a = A_k^{-1}(B_k + \bar{N}_k \lambda_k^n + \bar{D}_k \lambda_k^t) \tag{30}$$

Similar to (27), here, we adopt the velocity-level constraint. We can then write the following complementarity conditions Lloyd (2005):

$$0 \leq \sigma_k^n \perp \lambda_k^n \geq 0 \tag{31}$$

$$0 \leq \sigma_k^t \perp \lambda_k^t \geq 0 \tag{32}$$

$$0 \leq \sigma_k^f \perp \lambda_k^f \geq 0 \tag{33}$$

where

$$\begin{aligned} \sigma_k^n &:= \bar{N}_k^T \hat{V}_k^a \in \Re^{l_c} \\ \sigma_k^t &:= \bar{D}_k^T \hat{V}_k^a + U\lambda_k^f \in \Re^{l_c\times\bar{p}} \\ \sigma_k^f &:= \bar{\mu}\lambda_k^n - U^T \lambda_k^t \in \Re^{l_c} \end{aligned}$$

with $\bar{\mu} := \mu I_{l_c\times l_c}$ and $U := \mathrm{diag}[1_{\bar{p}}, 1_{\bar{p}}, ...1_{\bar{p}}] \in \Re^{(l_c\times\bar{p})\times\bar{p}}$. Here, (31) and (32) respectively specify the complementarity conditions along the normal and tangential directions, whereas (33) the Coulomb friction model with the friction cannot exceed $\mu\lambda^n$. Injecting (30) into (31)-(33), we can then attain the following PMI-LCP (linear complementarity problem) contact formulation:

$$\begin{aligned} &\begin{pmatrix} \sigma_k^n \\ \sigma_k^t \\ \sigma_k^f \end{pmatrix} = \begin{bmatrix} \bar{N}_k^T A_k^{-1} \bar{N}_k & \bar{N}_k^T A_k^{-1} \bar{D}_k & 0 \\ \bar{D}_k^T A_k^{-1} \bar{N}_k & \bar{D}_k^T A_k^{-1} \bar{D}_k & U \\ \mu I_{l_c\times l_c} & -U^T & 0 \end{bmatrix} \begin{pmatrix} \lambda_k^n \\ \lambda_k^t \\ \lambda_k^f \end{pmatrix} + \begin{pmatrix} \gamma_k^n \\ \gamma_k^t \\ 0 \end{pmatrix} \\ &\sigma_k^n, \sigma_k^t, \sigma_k^f, \lambda_k^n, \lambda_k^t, \lambda_k^f \geq 0 \\ &\sigma_k^{nT} \lambda_k^n = \sigma_k^{tT} \lambda_k^t = \sigma_k^{fT} \lambda_k^f = 0 \end{aligned} \tag{34}$$

where $\gamma_k^n := \bar{N}_k^T A_k^{-1} B_k$ and $\gamma_k^t = \bar{D}_k^T A_k^{-1} B_k$. This contact PMI-LCP (34) can be solved by using the interior point method or Lemke pivoting algorithm (Cottle et al. (2009)).

The complementarity conditions (31)-(33) naturally suggest passivity of our contact PMI-LCP formulation (34), i.e., lossless if no tangential slip occurs or dissipative if it occurs. This passivity of PMI-LCP (34) is clearly exhibited in Fig. 6, where a rigid box is free falling on a rigid level surface and bounces back and forth from that, with the total energy being constant during the flight stages, while strictly decreasing during the contact stages, during which dissipative tangential slips occur. Note that this simulates lossless (i.e., elastic) collision along the normal direction, whereas dissipative slips along the tangential directions, with no deformation allowed between the two rigid objects. With no slips, this would result in completely lossless/elastic collision.

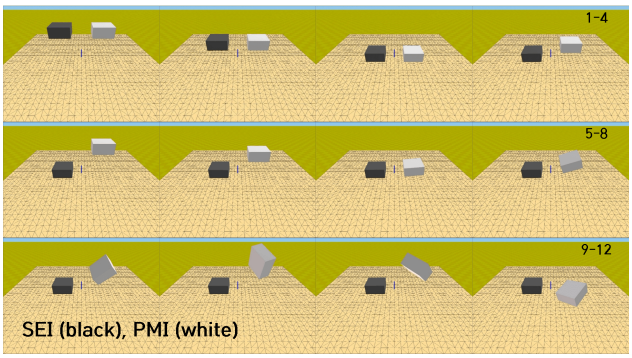

Figure 5. Snapshots of rigid box falling on rigid level surface: it bounces back and forth under PMI-LCP (white box), whereas completely plastically collides under SEI (black box) even with the same parameter setting.

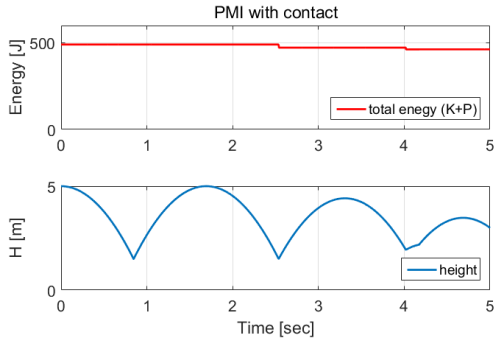

Figure 6. Profiles of total energy and height with PMI-LCP (34): elastic-normal and dissipative-tangential slips contact attained with total energy remained constant during flight, whereas strictly decreased during contact. Sudden changes of H around 4-4.2[sec] are due to collision with flipping.

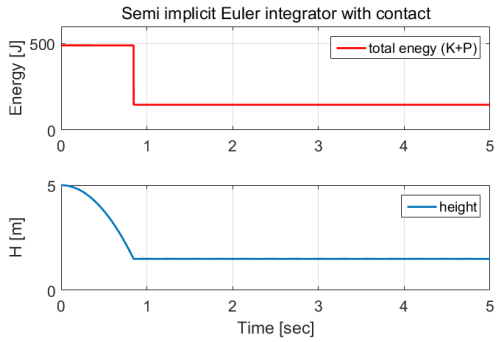

Figure 7. Profiles of total energy and height with SEI: although the setting is the same as Fig. 6, completely plastic collision is attained (see also Fig. 5).

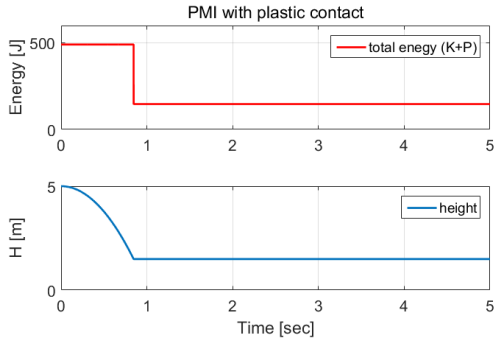

Figure 8. Profiles of total energy and height under PMI-LCP (34) with $\hat{V}_k^a$ replaced by V_{k+1} for (31)-(32): completely plastic collision attained as in Fig. 7 under SEI.

This ability of our PMI-LCP (34) to naturally render (marginally-stable) elastic contact is in a stark contrast to other contact rendering results based on IEI or SEI, which typically can only produce plastic contact unless some extra velocity restitution models are deployed. This is in fact due to the adoption of v_{k+1} as the representative velocity by the IEI and SEI (see Sec. 2.3). See Fig. 7, where the same box-falling scenario of Fig. 6 results in purely plastic collision with the SEI. Of course, in many applications, plastic collisions are necessary, which can also be easily achieved by our PMI-LCP (34) simply replacing $\hat{V}_k^a$ in σ_k^n, σ_k^t by V_{k+1} - see Fig. 8.

Here, note that, in contrast to that of Sec. 3.2 (i.e., approximate passivity of λ_k (25)), this passivity of the PMI-LCP is exact, since we do not adopt such a Jacobian approximation as done in (22). Consequently, the damping injection, added to enforce passivity of the approximate potential action in Sec. 3.2, is not necessary here either. Our PMI-LCP algorithm is formulated at the velocity-level (i.e., (27)), thus, suffers from the issue of constraint drift (induced by initial collision detection error or numerical precision error). This constraint drift can be easily remedied by incorporating some drift-correction term into γ_k^n of (34) as similarly done in Otaduy et al. (2009). Another interesting direction for this is to combine the PMI-LCP formulation with the approximate action of the potential ψ_{λ_k} of Sec. 3.2 to stabilize this constraint drift. Passivity (thus, stability) of these drift-correction or combining the PMI-LCP with its approximate constraint potential, however, has not been established and is a topic for future research.

4. PMI-Based Simulation in Generalized Coordinates

In this Sec. 4, we derive the PMI of the Lagrange dynamics (4) in generalized coordinates. We first show that the PMI formulation developed in Sec. 2.2 and Sec. 3.1 are not able to enforce passivity for the Lagrange dynamics (4) due to the dynamics nonlinearity. To overcome this, we then propose a certain coordinate transformation, with which the nonlinear Lagrange dynamics (4) can be converted into the form amicable for the PMI formalism to enforce passivity in the discrete-time domain. We further show how to derive the PMI-LCP formulation in generalized coordinates for the Lagrange dynamics (4) to simulate point Coulomb friction contact, as done so in Sec. 3.3 for the PMI in maximal coordinates.

4.1. PMI of Lagrange Dynamics

Consider the multi-DOF nonlinear Lagrange dynamics (4) with the generalized coordinates $q \in \Re^n$. Here, we focus on quadratic potential functions $\psi(q) = \frac{1}{2} q^T K q$, since, with them, we can establish discrete-time passivity exactly with no approximations necessary. Of course, other types of analytic nonlinear potentials $\psi(q)$ can also be used in the same manner, with their potential action approximated as in Sec. 3.2 to preserve the non-iterativeness of the PMI simulation and with some damping B injection to enforce

the discrete-time passivity even with this approximation. Contacts with external objects, whose position can possibly be nonlinear w.r.t. q (i.e., on-link contact), are to be rendered by PMI-LCP formulation of Sec. 4.3 via f_c in (4) instead of via the potential $\psi(q)$.

Now, suppose $M(q)$ in (4) be constant (i.e., $M(q) = M$). This means $C(q, \dot{q})$ in (4) is skew-symmetric, since $\dot{M} - 2C$ is skew-symmetric. We can then write the PMI expression of (4) as a vector version of (9), with x_k, v_k replaced by $q_k, v_k := \dot{q}_k \in \Re^n$ and also with $C_k\hat{v}_k := C(q_k, v_k)\hat{v}_k$ added in (9) similar to the term $S(Jw_k)\hat{w}_k$ in (13). Further, similar to (15), we can show that this PMI of Lagrange dynamics (4) with constant M and linear spring potential $d\psi_k^T = Kq_k$ is discrete-time passive, i.e., $\forall N \geq 1$,

$$\sum_{k=0}^{N-1}[f_k + f_k^c]^T\hat{v}_k T_k = \sum_{k=0}^{N-1}\left[E_{k+1} - E_k + \hat{v}_k^T C_k\hat{v}_k T_k\right] = E_{\bar{N}+1} - E_o \geq -E_o \tag{35}$$

where C_k is skew-symmetric, $\hat{v}_k := (v_{k+1} + v_k)/2$ is the "representative" velocity during T_k, and $E_k := \frac{1}{2}v_k^T M v_k + \frac{1}{2}q_k^T K q_k$ is the total energy.

This discrete-time passivity (35), however, is not granted for non-constant M. That is, from $M(q)$ being configuration-dependent, we have $M_{k+1} := M(q_{k+1}) \neq M_k := M(q_k)$, with which, instead of (35), we have:

$$\sum_{k=0}^{N-1}[f_k^c + f_k]^T\hat{v}_k T_k = \frac{1}{2}q_N^T K q_N - \frac{1}{2}q_o^T K q_o + \sum_{k=0}^{N-1}\left[\frac{v_{k+1}^T M_k v_{k+1}}{2} - \frac{v_k^T M_k v_k}{2} + \hat{v}_k^T C_k\hat{v}_k T_k\right]$$

where, differently from (35), the kinetic energies in the bracket do not cancel out with each other over the successive T_k and T_{k+1}, and C_k is not skew-symmetric either. This is because the skew-symmetricity of $\dot{M} - 2C$ (or, equivalently, $\dot{M} = C + C^T$) cannot be simulated during T_k, since doing so requires future information M_{k+1}, C_{k+1} at the onset of T_k. To address this, here, we utilize the coordinate transformation proposed in (Lee et al. (2012)), with which the nonlinear Lagrange dynamics (4) is transformed into another Lagrangian form with constant inertia and skew-symmetric Coriolis term, thus, can still be passively by using PMI similar to (13).

More precisely, define the following (continuous-time) coordinate transformation:

$$\xi := M^{\frac{1}{2}}(q)\dot{q}, \quad \delta := M^{-\frac{1}{2}}(q)f \tag{36}$$

with which the kinetic energy can be written as

$$\frac{1}{2}\dot{q}^T M(q)\dot{q} = \frac{1}{2}\xi^T I \xi$$

where $I \in \Re^{n\times n}$ is the identity matrix, implying that, for the transformed velocity ξ, the inertia will be this constant I. Using

$$I\dot{\xi} = M^{\frac{1}{2}}(q)\ddot{q} + \tfrac{d}{dt}[M^{\frac{1}{2}}(q)]\dot{q}$$

we can then rewrite (4) s.t.

$$I\dot{\xi} + Q(q, \dot{q})\xi + M^{-\frac{1}{2}}(q)Kq = \delta_c + \delta \tag{37}$$

where the Coriolis-like term $Q(q, \dot{q}) \in \Re^{n\times n}$ is defined by

$$Q(q, \dot{q}) := M^{-\frac{1}{2}}CM^{-\frac{1}{2}} - \tfrac{d}{dt}[M^{\frac{1}{2}}]M^{-\frac{1}{2}} \tag{38}$$

with arguments omitted for brevity.

This matrix Q in (38) is in fact skew-symmetric. That is, with M being symmetric, we have

$$\begin{aligned} Q + Q^T &= M^{-\frac{1}{2}}[C + C^T]M^{-\frac{1}{2}} - \tfrac{d}{dt}[M^{\frac{1}{2}}]M^{-\frac{1}{2}} - M^{-\frac{1}{2}}\tfrac{d}{dt}[M^{\frac{1}{2}}] \\ &= M^{-\frac{1}{2}}\tfrac{d}{dt}[M^{\frac{1}{2}}M^{\frac{1}{2}}]M^{-\frac{1}{2}} - \tfrac{d}{dt}[M^{\frac{1}{2}}]M^{-\frac{1}{2}} - M^{-\frac{1}{2}}\tfrac{d}{dt}[M^{\frac{1}{2}}] \\ &= 0 \end{aligned}$$

where we use the fact that $\dot{M} = C + C^T$ from $\dot{M} - 2C$ being skew-symmetric. We can also show that the transformed dynamics (37) preserves the same passivity as (5): $\forall T \geq 0$,

$$\begin{aligned} \int_0^T [f_c + f]^T\dot{q}dt &= \int_0^T [\delta_c + \delta]^T\xi dt \\ &= \int_0^T \left[\xi^T I\dot{\xi} + \xi^T Q\xi + \xi^T M^{-\frac{1}{2}}Kq\right]dt \\ &= E(T) - E(0) \geq -E(0) \end{aligned}$$

where $E := \frac{1}{2}\dot{q}^T M(q)\dot{q} + \frac{1}{2}q^T Kq = \frac{1}{2}\xi^T I\xi + \frac{1}{2}q^T Kq$ is the total energy.

Since the transformed dynamics (37) has constant inertia I and skew-symmetric Q, we can now passively simulate (37) similar to (9) and (13) s.t.

$$I\frac{\xi_{k+1} - \xi_k}{T_k} + Q_k\frac{\xi_{k+1} + \xi_k}{2} + M_k^{-\frac{1}{2}}K\frac{q_{k+1} + q_k}{2} = \delta_{c_k} + \delta_k \tag{39}$$

where $\delta_{c_k} := M_k^{-\frac{1}{2}}f_{c_k}$, $\delta_k := M_k^{-\frac{1}{2}}f_k$, and $Q_k := Q(q_k, v_k)$. We can then show that

$$\begin{aligned} &\sum_{k=1}^{N-1}[\delta_{c_k} + \delta_k]^T\hat{\xi}_k T_k \\ &= \sum_{k=0}^{N-1}\left[\kappa_{k+1} - \kappa_k + \hat{\xi}_k^T Q_k\hat{\xi}_k T_k + \hat{\xi}_k^T M_k^{-\frac{1}{2}}K\frac{q_{k+1} + q_k}{2}T_k\right] \\ &= \kappa_N - \kappa_o + \sum_{k=0}^{N-1}\hat{\xi}_k^T M_k^{-\frac{1}{2}}K\frac{q_{k+1} + q_k}{2}T_k \end{aligned}$$

where $\hat{\xi}_k := (\xi_{k+1} + \xi_k)/2$, $\kappa_k := \xi_k^T I\xi_k/2 = v_k^T M_k v_k/2$, and we use the fact that Q_k is skew-symmetric. This then also suggests the following kinematics law, similar to (8), yet, transformed via $M_k^{\frac{1}{2}}$, s.t.

$$\frac{q_{k+1} - q_k}{T_k} = M_k^{-\frac{1}{2}}\frac{\xi_{k+1} + \xi_k}{2} \tag{40}$$

which is indeed consistent with the continuous-time transformation (36).

Note that, given the continuous-time Lagrangian dynamics (4), we first transform it to (37); then discretize it via (39); and connect to the configuration q of the original dynamics through (40). To compute Q_k via (38), we may also use

the following (discrete-time) Sylvester equation (Horn and Johnson 2012) to obtain $\dot{M}_k^{\frac{1}{2}}$, that is, given $M_k^{\frac{1}{2}}, C_k$, find $\dot{M}_k^{\frac{1}{2}}$ s.t.,

$$\dot{M}_k^{\frac{1}{2}} M_k^{\frac{1}{2}} + M_k^{\frac{1}{2}} \dot{M}_k^{\frac{1}{2}} = \dot{M}_k = [C_k + C_k^T]$$

with which we can also show that $Q_k = M_k^{-\frac{1}{2}} C_k M_k^{-\frac{1}{2}} - \dot{M}_k^{\frac{1}{2}} M_k^{-\frac{1}{2}}$ is skew-symmetric. In the next Sec. 4.3, we will explain how to render the contact force δ_{c_k} in (39) based on the point contact Coulomb friction model by incorporating LCP (linear complementarity problem) formulation into the PMI expression (39) as similarly done in Sec. 3.3. Before doing so, let us first compare the PMI with symplectic integrators to shed light to some unique and useful properties of the PMI.

4.2. Comparison of PMI with Symplectic Integrators

To define symplectic integrators for the Lagrangian dynamics (4), let us define its Hamiltonian s.t.,

$$H(p,q) = p^T M(q)^{-1} p + U(q)$$

where $q \in \Re^n$ is the configuration, $p := M(q)\dot{q} \in \Re^n$ is the conjugate momenta, and $U(q) \in \Re$ is the potential energy. Then, the Hamiltonian dynamics formulation of (4) is given by

$$\dot{p} = -\frac{\partial H}{\partial q}(p,q), \quad \dot{q} = \frac{\partial H}{\partial p}(p,q)$$

which can be written in the following matrix form:

$$\dot{y} := \begin{pmatrix} \dot{p} \\ \dot{q} \end{pmatrix} = \begin{bmatrix} 0 & I \\ -I & 0 \end{bmatrix}^{-1} \begin{pmatrix} \frac{\partial H}{\partial p} \\ \frac{\partial H}{\partial q} \end{pmatrix} =: \mathsf{J}^{-1} \cdot \nabla H(y) \quad (41)$$

where $y := [p; q] \in \Re^{2n}$ is the coordinate in the tangent bundle, $\nabla H(y) = [\frac{\partial H}{\partial p}; \frac{\partial H}{\partial q}] \in \Re^{2n}$ is the gradient of H, and $\mathsf{J} \in \Re^{2n \times 2n}$ is the (skew-symmetric) canonical structure matrix. The solution of the Hamiltonian system (41) can then be written by its flow map ψ_t with $\psi_t(y_0) := y(t, y_0)$.

Three fundamental properties the Hamiltonian system (41) possesses, namely, energy conservation (or passivity), momentum conservation and symplecticity. Since the first two are familiar, we explain here only the symplecticity. A linear mapping $A : \Re^{2n} \to \Re^{2n}$ is called *symplectic* if

$$w(A\zeta_1, A\zeta_2) = w(\zeta_1, \zeta_2) \quad (42)$$

for $\zeta_1 := [\zeta_1^p, \zeta_1^q], \zeta_2 := [\zeta_2^p, \zeta_2^q] \in \Re^{2n}$ with $\zeta_1^p, \zeta_1^q, \zeta_2^p, \zeta_2^q \in \Re^n$, where

$$w(\zeta_1, \zeta_2) := \sum_{i=1}^{n} \det \begin{pmatrix} \zeta_{1,i}^p & \zeta_{2,i}^p \\ \zeta_{1,i}^q & \zeta_{2,i}^q \end{pmatrix} = \sum_{i=1}^{n} (\zeta_{1,i}^p \zeta_{2,i}^q - \zeta_{1,i}^q \zeta_{2,i}^p)$$

which is the sum of the oriented areas, i.e., symplecticity implies the area preservation through the map A. For the Hamiltonian system (41), the symplecticity condition is given by

$$\left(\frac{\partial \psi_t}{\partial y_0}\right)^T \mathsf{J} \left(\frac{\partial \psi_t}{\partial y_0}\right) = \mathsf{J}$$

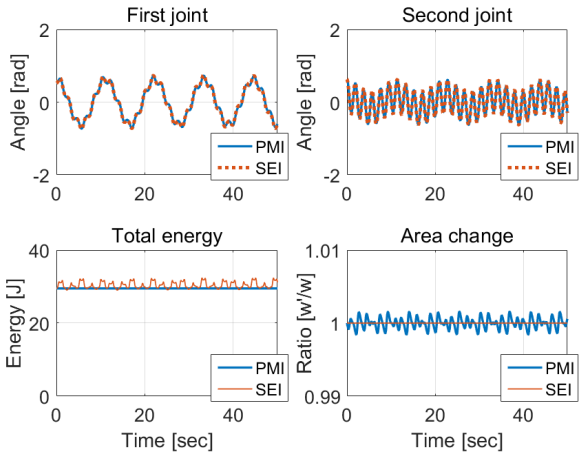

Figure 9. Simulation of two serial-link robot arm with linear joint springs with SEI and PMI: the SEI is symplectic, yet, not exactly energy-preserving, whereas the PMI is energy-preserving, yet, not exactly symplectic.

Symplectic integrators are those that preserve this simplecticity property of the continuous-time Hamiltonian system (41). The following symplectic Euler integration (SEI) and implicit midpoint integration (IMI) are those symplectic integrators

$$y_{k+1} = y_k + \mathsf{J}^{-1} \cdot \nabla H(p_{k+1}, q_k) T$$
$$y_{k+1} = y_k + \mathsf{J}^{-1} \cdot \nabla H(p_k, q_{k+1}) T \quad (43)$$
$$y_{k+1} = y_k + \mathsf{J}^{-1} \cdot \nabla H(\hat{p}_k, \hat{q}_k) T \quad (44)$$

with the first two being the SEI and the last the IMI, where $y_k := [p_k; q_k] \in \Re^{2n}$, $T > 0$ is the integration step, and $\hat{\star}_k := \frac{\star_{k+1} + \star_k}{2}$. Both of these SEI and IMI are known to be symplectic and momentum conserving, yet, not energy preserving, where the symplecticity condition is given by

$$\left(\frac{\partial y_{k+1}}{\partial y_k}\right)^T \mathsf{J} \left(\frac{\partial y_{k+1}}{\partial y_k}\right) = \mathsf{J} \quad (45)$$

Now, let us see if the PMI (39)-(40) is also symplectic. For this, from (39)-(40), we can obtain the following equation:

$$\begin{pmatrix} p_{k+1} \\ q_{k+1} \end{pmatrix} = \begin{bmatrix} M_{k+1}^{\frac{1}{2}}(q_{k+1}) & 0 \\ 0 & I \end{bmatrix} \left(\frac{I}{T_k} + S_k(p_k, q_k)\right)^{-1} \times \left(\frac{I}{T_k} - S_k(p_k, q_k)\right) \begin{bmatrix} M_k^{-\frac{1}{2}}(q_k) & 0 \\ 0 & I \end{bmatrix} \begin{pmatrix} p_k \\ q_k \end{pmatrix} \quad (46)$$

where $p_k = M^{\frac{1}{2}}(q_k)\xi_k \in \Re^n$ and $S_k(p_k, q_k) := \frac{1}{2}\left[Q_k(p_k, q_k), M_k^{-\frac{1}{2}}(q_k)K;\ M_k^{-\frac{1}{2}}(q_k), 0\right] \in \Re^{2n \times 2n}$.

To derive (45) from (46) turns out too complicated to analytically perform. Note however that we have $M_{k+1}^{\frac{1}{2}}$ in (46), which, in general, can take any positive definite matrix, suggesting the PMI would be unlikely symplectic. For this, here, we resort to a numerical approach, that is, measure how the area of a certain shape in the space of $(p, q) \in \Re^{2n}$ evolves in the course of the PMI integration of (39)-(40). The results are shown in Fig. 9, where we can see that the PMI is energy-preserving (from passivity), yet, not symplectic,

although it still stays near to be symplectic. We can show that the PMI is not momentum-preserving either. This then means that the PMI is not the IMI, although, for linear mechanical systems, they become the same.

Even so, we believe the PMI has advantages for haptic rendering and interactive simulation as compared to those symplectic integrators particularly due to the following two powerful properties: 1) non-iterativeness and 2) passivity. Note first from (43)-(44) that the symplectic integrators should in general solve the nonlinear map (i.e., ∇H) real-time in an iterative manner due to the presence of the same variables both in the left-hand side and inside of $\nabla H(\star)$ in (43)-(44). This iterative nature of the symplectic integrators, combined with their non-passivity (i.e., instability possible), poses a challenging issue in practice, that is, this nonlinear map must be solved precisely to maintain stability, which may be time-consuming for complex ∇H or requires only small time-step T to ensure fast-enough convergence of this nonlinear map solving, both not so suitable for real-time interactivity of simulation. From its being dissipative, the IEI, in contrast, is known to be less sensitive to this solution precision and often chosen over the SEI or IMI when this issue becomes important.

On the other hand, note from (26) or (39)-(40) that the PMI is non-iterative with no necessity to solve such a nonlinear map. This non-iterativeness of the PMI is attained due to the coordinate transformation (36) (for nonlinearity from inertia) and the potential action approximation (e.g., (24) for potential nonlinearity). Of course, with this approximate action of nonlinear potentials, the passivity will be also in general only approximate. This "leakage" of passivity, yet, can be rather easily resolved by injecting (typically small) linear damping B, which can be still simulated quickly due to the non-iterativeness of the PMI and whose passivity also still guaranteed due to the passivity of the PMI. This unconditionally stable/passive damping allows for the so called "controllable damping" (e.g., increase (or decrease, resp.) B for more stable (or less stable, resp.) behaviors while preserving simulation stability), which is not possible for those symplectic integrators, theoretically or practically (i.e., precision of nonlinear map solving). These non-iterativeness and passivity, we believe, are more relevant than symplecticity and momentum-preserving for haptic rendering and interactive simulation, since the stability and real-time interactivity are their most fundamental requirements and their simulated objects are also anyway typically under the influence of frequent human/contact forces differently from those in celestial mechanics or molecular simulation, where long-term isolated behavior simulation is more important.

4.3. PMI-LCP for Multi-Point Coulomb Friction Contact

Following the procedure of Sec. 3.3, here, we utilize the point contact model with Coulomb friction. Here, we assume the multi-DOF Lagrange system (39) interacts with a static virtual rigid object. We choose here this static object for simplicity: the derivation presented below can be easily applied to multiple moving rigid objects, which can then be rendered by using the PMI expression in maximal coordinates of Sec. 3. We also adopt the velocity level complementary condition as in (27) and the $\bar{p}$-pyramidal cone approximation as in (29), and denote by l_c the number of contact points between the Lagrange system (39) and the object.

Then, the contact force $\delta^c_{i,k} \in \Re^n$ at the i-th contact point ($i \in \{1, 2, ..., l_c\}$) can be written by

$$\delta^c_{i,k} = M_k^{-\frac{1}{2}} f^c_{i,k} = M_k^{-\frac{1}{2}} J^T_{c_i,k} \left[N_{i,k}\lambda^n_{i,k} + D_{i,k}\lambda^t_{i,k} \right] \quad (47)$$

where $J_{c_i,k}(q_k) \in \Re^{3\times n}$ is the Jacobian of the i-th contact point, and $\lambda^n_{i,k} \in \Re$ and $\lambda^t_{i,k} \in \Re^{\bar{p}}$ are the normal contact and tangential friction forces with $N_{i,k} \in \Re^3$ and $D_{i,k} \in \Re^{3\times\bar{p}}$ respectively encoding their directions in $\Re^3$, defined in a manner similar to (29). Combining (47) for all the l_c contact points, we can then obtain the total contact force δ_{c_k} in (39) s.t.,

$$\delta_{c_k} = \bar{N}_k\lambda^n_k + \bar{D}_k\lambda^t_k$$

where

$$\begin{aligned}
&\lambda^n_k := [\lambda^n_{1,k}; \lambda^n_{2,k}; ...; \lambda^n_{l_c,k}] \in \Re^{l_c} \\
&\lambda^t_k := [\lambda^t_{1,k}; \lambda^t_{2,k}; ...; \lambda^t_{l_c,k}] \in \Re^{l_c\times\bar{p}} \\
&\bar{N}_k := M_k^{-\frac{1}{2}} \left[J^T_{c_1,k}N_{1,k}, J^T_{c_2,k}N_{2,k}, ...J^T_{c_{l_c},k}N_{l_c,k} \right] \in \Re^{n\times l_c} \\
&\bar{D}_k := M_k^{-\frac{1}{2}} \left[J^T_{c_1,k}D_{1,k}, J^T_{c_2,k}D_{2,k}, ...J^T_{c_{l_c},k}D_{l_c,k} \right] \in \Re^{n\times(l_c\times\bar{p})}
\end{aligned}$$

with which we can also rewrite the PMI expression of the Lagrange dynamics (39) similar to (30), i.e.,

$$\hat{\xi}_k = A_k^{-1} \left[B_k + \bar{N}_k\lambda^n_k + \bar{D}_k\lambda^t_k \right] \quad (48)$$

where $A_k := \frac{2}{T_k} I + Q_k + \frac{1}{2} M_k^{-\frac{1}{2}} K M_k^{-\frac{1}{2}} T_k$ and $B_k := \frac{2}{T_k}\xi_k - M_k^{-\frac{1}{2}} K q_k$.

Given this $\hat{\xi}_k$ in (48), we can compute the velocity of all the l_c contact points s.t.,

$$\hat{V}^c_k = J_{c_k} M_k^{-\frac{1}{2}} \hat{\xi}_k \in \Re^{3l_c} \quad (49)$$

where $J_{c_k} := \left[J_{c_1,k}; J_{c_2,k}; ...J_{c_{l_c},k} \right] \in \Re^{3l_c\times n}$ is the combined Jacobian of the l_c contact points. The contact complementarity conditions (Lloyd (2005)) can be written similar to (31)-(33) s.t.,

$$\begin{aligned}
0 \le \sigma^n_k \perp \lambda^n_k \ge 0 \\
0 \le \sigma^t_k \perp \lambda^t_k \ge 0 \\
0 \le \sigma^f_k \perp \lambda^f_k \ge 0
\end{aligned}$$

where

$$\begin{aligned}
&\sigma^n_k := N_k^T \hat{V}^c_k \in \Re^{l_c} \\
&\sigma^t_k := D_k^T \hat{V}^c_k + U\lambda^f_k \in \Re^{l_c\times\bar{p}} \\
&\sigma^f_k := \bar{\mu}\lambda^n_k - U^T\lambda^t_k \in \Re^{l_c}
\end{aligned}$$

where $N_k := \mathrm{diag}[N_{1,k}, N_{2,k}, ...N_{l_c,k}] \in \Re^{3l_c\times l_c}$, $D_k := \mathrm{diag}[D_{1,k}, D_{2,k}, ...D_{l_c,k}] \in \Re^{3l_c\times(l_c\times\bar{p})}$, and $\bar{\mu} := \mu I_{l_c\times l_c}$ and $U := \mathrm{diag}[1_{\bar{p}}, 1_{\bar{p}}, ..1_{\bar{p}}] \in \Re^{(l_c\times\bar{p})\times\bar{p}}$ as for (31)-(33).

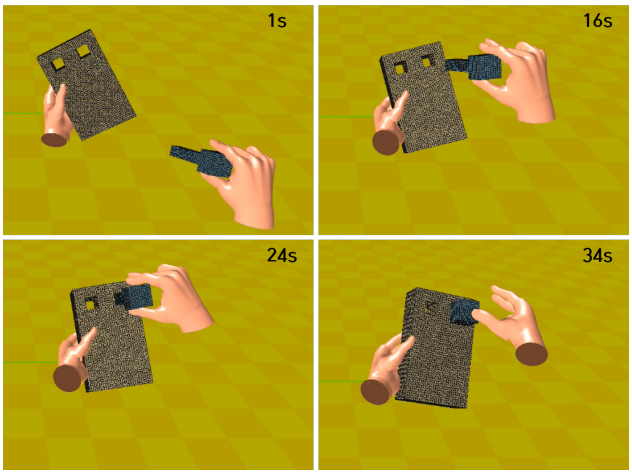

Figure 10. Snapshots of peg-in-hole task with two multi-fingered hands, each modeled as articulated rigid bodies as shown in Fig. 4 and making contact with the objects via friction contact simulated by PMI-LCP of Sec. 3.3.

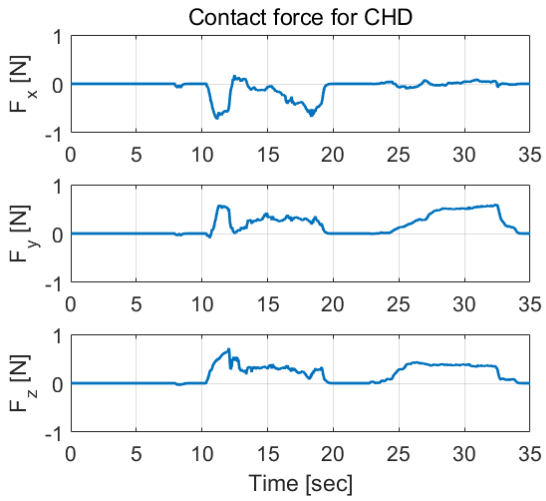

Figure 11. Finger-tip contact force during the peg-in-hole task of Fig. 10 expressed in the finger-tip coordinate frame (with z-axis being the contact normal direction).

Finally, similar to (34), we can construct the PMI-LCP formulation in generalized coordinates s.t.,

$$\begin{pmatrix}\sigma_k^n\\ \sigma_k^t\\ \sigma_k^f\end{pmatrix} = \begin{bmatrix} W_{11} & W_{12} & 0\\ W_{21} & W_{22} & U\\ \mu I_{l_c\times l_c} & -U^T & 0\end{bmatrix}\begin{pmatrix}\lambda_k^n\\ \lambda_k^t\\ \lambda_k^f\end{pmatrix} + \begin{pmatrix}\gamma_k^n\\ \gamma_k^t\\ 0\end{pmatrix}$$
$$\sigma_k^n, \sigma_k^t, \sigma_k^f, \lambda_k^n, \lambda_k^t, \lambda_k^f \geq 0$$
$$\sigma_k^{nT}\lambda_k^n = \sigma_k^{tT}\lambda_k^t = \sigma_k^{fT}\lambda_k^f = 0 \qquad (50)$$

where $\gamma_k^n := N_k^T J_{c_k} M_k^{-\frac{1}{2}} A_k^{-1} B_k$, $\gamma_k^t := D_k^T J_{c_k} M_k^{-\frac{1}{2}} A_k^{-1} B_k$ and

$$W_{11} := N_k^T J_{c_k} M_k^{-\frac{1}{2}} A_k^{-1} M_k^{-\frac{1}{2}} J_{c_k}^T N_k$$
$$W_{12} := N_k^T J_{c_k} M_k^{-\frac{1}{2}} A_k^{-1} M_k^{-\frac{1}{2}} J_{c_k}^T D_k = W_{21}^T$$
$$W_{22} := D_k^T J_{c_k} M_k^{-\frac{1}{2}} A_k^{-1} M_k^{-\frac{1}{2}} J_{c_k}^T D_k$$

which can be solved by interior point method or Lemke's pivoting algorithm (Cottle et al. (2009)).

5. Illustrative Examples

So far, we have derived the PMI-based simulation framework, which, due to its enforcing passivity effective in practice, can stably simulate wide-range of parameters (e.g., very light/stiff objects with no damping) regardless of (possibly varying/slow) integration steps T_k, that can occur during, e.g., intermittent multi-point collisions among virtual objects. To validate and demonstrate these (and other) advantages of our proposed PMI-based simulation framework, here, we perform three illustrative examples, namely, haptic operation of peg-in-hole task (Sec. 5.1), haptic interaction with flexible beam (Sec. 5.2), and multi-point power grasping of multi-fingered under-actuated tendon-drive (UATD) hand (Sec. 5.3).

5.1. Peg-in-Hole Task

For the peg-in-hole task, we model the peg and the box with holes as rigid bodies, whereas the two multi-fingered virtual hand as articulated rigid bodies with joint constraints as shown in Fig. 4, each composed of ten articulated rigid bodies. To simulate these, we apply the PMI-based formulation in maximal coordinates of Sec. 3. We also utilize the wearable cutaneous haptic device proposed in (Kim et al. 2016), which can provide 3-DOF contact force feedback at the finger-tip. This cutaneous haptic device is different from typical haptic devices (e.g., Omega 3, Geomagic Phantom), as it cannot generate kinesthetic force feedback. Consequently, we utilize the unilateral virtual couping to allow the user to command the position/orietation of the virtual hands/fingers, whereas the finger-tip contact force is directly fed back to the cutaneous haptic device.

More precisely, the SE(3) springs, consisting of E(3) linear spring of Sec. 2.2 and SO(3) spring of Sec. 3.1, are used as uni-directional position/orientation-commanding virtual coupling (e.g., Lee (2009); Kim and Lee (2017)). On the other hand, the contact force of each finger-tip of the virtual hands during the manipulation (computed via PMI-LCP of Sec. 3.3) is directly fed back to the cutaneous finger-tip haptic device. For this, we use

$$f_{f,k} = R_{f,k}^T H_{\text{filter}}(f_{i,k-1}^c, f_{i,k-2}^c, \ldots f_{i,k-p_f}^c)$$

where $R_{f,k}$ is the rotation matrix of the finger-tip body frame w.r.t. the inertial frame, and H_{filter} is a certain low-pass-filter to process the p_f-number of the computed contact force data $f_{i,k-j}^c$, $j = 1, \ldots, p_f$. The filter H_{filter} is used here to provide smooth cutaneous haptic feedback $f_{f,k}$ (with 1kHz) from the computed contact force $f_{i,k}^c$, whose update-rate is varying between 30-300Hz due to the simulation of the large number of rigid bodies (i.e., two hands, each composed of 10 rigid bodies, one box with holes, and one peg) and multi-point contacts among them. Note that we cannot use $f_{i,k}^c$ for H_{filter}, since it can be determined only after $T_k = [t_k, t_{k+1})$. The computational-lag from H_{filter} and the uni-laterality of the virtual coupling do not affect stability, since the device-human coupling here is only cutaneous, not kinesthetic (Prattichizzo et al. 2013).

Snapshots of this peg-in-hole task are shown in Fig. 10 with its finger-tip forces also presented in Fig. 11. We set the

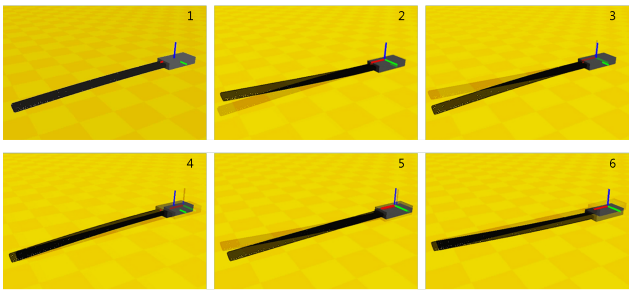

Figure 12. Snapshots of PMI-based simulation of undamped flexible beam harmonic oscillation.

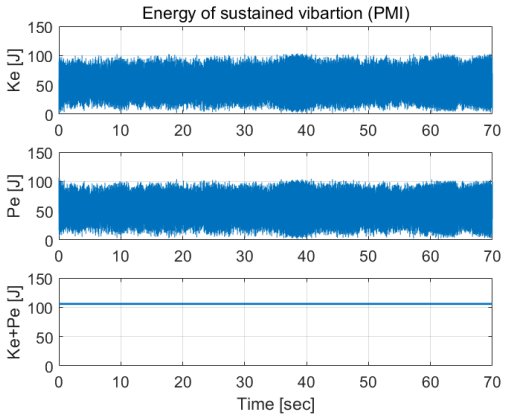

Figure 13. Profiles of kinetic, potential and total energies of the PMI-based simulation of undamped flexible beam vibration in Fig. 12: note the exact conservation of total energy during the fast oscillations.

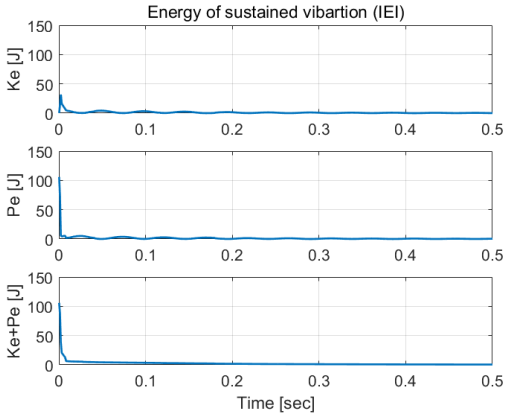

Figure 14. Profiles of kinetic, potential and total energies of the IEI-based simulation of undamped flexible beam vibration in Fig. 12 with linearized inertia matrix: note the total energy quickly decays due to dissipativity of the IEI, although the same initial conditions as that of Fig. 13 are used.

mass/inertia of rigid bodies of the hand as $m = 0.001$[kg] and $J = mI_{3\times3}$[kgm^2], while the stiffness of the spring stiffness as $k_\lambda = 100$[N/m], with the stiffness/mass ratio to be fairly high of 10^5. We found that, with these parameters, the cutaneous haptic feedback rendering is transparent enough, since: 1) the virtual hand can (unilaterally) follow the user command fast enough with this high stiffness/mass ratio of 10^5; and 2) the cutaneous force feedback $f_{f,k}$, as computed above, is directly displayed to the finger-tip with no intermediate compliance. Note that this differs from the case of kinesthetic devices with bilateral virtual coupling, where, for the transparency, the virtual coupling should typically be much higher, as it defines bilateral compliant coupling between the virtual proxy and the real haptic device. Of course, we can also adopt kinesthetic haptic devices here along with, e.g., virtual coupling developed for the PMI (Huang and Lee 2011; Lee et al. 2012), or passive set-position modulation (PSPM: Lee and Huang (2010)). In this case, even if we use the PMI to enforce the passivity of the virtual worlds, the (hybrid/bilateral) virtual coupling gain will be still limited by the device physical damping - see (Huang and Lee 2011).

5.2. Haptic Interaction with Flexible Beam

We model the flexible beam to be an aluminum beam with the dimension of $(0.907, 0.05, 0.012)$[m] and the mass of 1.4683[kg]. We also model its dynamics by using nodal coordinates with three natural frequencies of $(11.91, 74.65, 209.03)$[Hz]. Here, for simplicity, we assume the beam motion to be planar. Then, the beam dynamics can be modeled in mixed maximal-generalized coordinates and using Euler-Bernoulli model (Rao and Yap (1995)) s.t.,

$$\begin{bmatrix} M_{xx} & M_{x\delta} \\ M_{\delta x} & M_{\delta\delta} \end{bmatrix} \begin{pmatrix} \ddot{x} \\ \ddot{\delta} \end{pmatrix} + \begin{bmatrix} C_{xx} & C_{x\delta} \\ C_{\delta x} & 0 \end{bmatrix} \begin{pmatrix} \dot{x} \\ \dot{\delta} \end{pmatrix} + d\psi^T(\delta) = f$$

where $x \in \Re^3$ is the maximal coordinate of the beam end in SE(2), $\delta \in \Re^3$ is the generalized coordinate representing each vibration mode, $d\psi^T(\delta) := K_q q := [0; K_{\delta\delta}\delta]$, where $M_{\delta\delta}, K_{\delta\delta} \in \Re^{3\times3}$ are the constant inertia and stiffness matrices of vibration. On the other hand, other matrices $M_\star, C_\star \in \Re^{3\times3}$ are configuration-dependent nonlinear inertia and Coriolis matrices, with the off-diagonal terms representing the dynamic coupling.

Snapshots and profiles of kinetic, potential and total energies of undamped vibration of this flexible beam simulated by our PMI-based framework with $x = 0$ are shown in Fig. 12 and Fig. 13, respectively, where the integration interval is 1kHz. There, we can see that the total energy is conserved throughout this fairly fast undamped vibration, clearly showing the ability of our PMI-based framework to simulate lossless/marginally-stable/energy-conserving behaviors. This undamped harmonic oscillation cannot be stably simulated by the SEI. It can however be done by the IEI, for which we must have adopted some linearization as introduced in Duriez et al. (2006); Courtecuisse et al. (2015) to render the IEI interactively-fast. The results with this IEI simulation are shown in Fig. 14, where it is clear that the IEI exhibits strictly-stable oscillation with the total energy quickly decaying to zero. This lack of ability to simulate lossless behaviors of the IEI is in fact due to its dissipativity (see Sec. 2.3), meaning that its advantage over our PMI framework is unclear, as the implementation complexity is at least comparable between PMI and IEI.

For the haptic interaction, we connect the flexible beam to a square rigid box via a spring, which is in turn connected to Omega 3® haptic device via virtual coupling (Lee et al. (2012)). See Fig. 15. The dynamics of the total system can

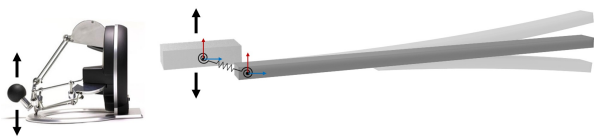

Figure 15. Flexible beam (in generalized coordinates) is connected to rigid body (in maximal coordinates) via spring, which is in turn connected to haptic device via virtual coupling.

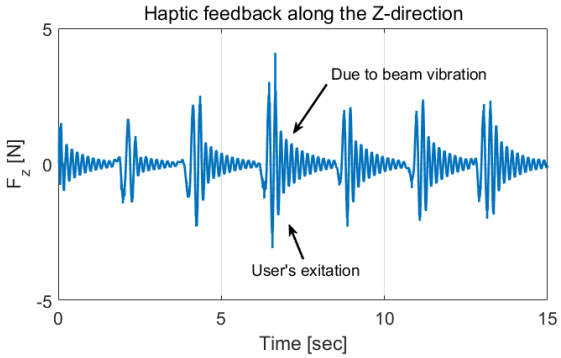

Figure 16. Haptic feedback from the flexible beam to the haptic device through virtual coupling connected to the rigid box.

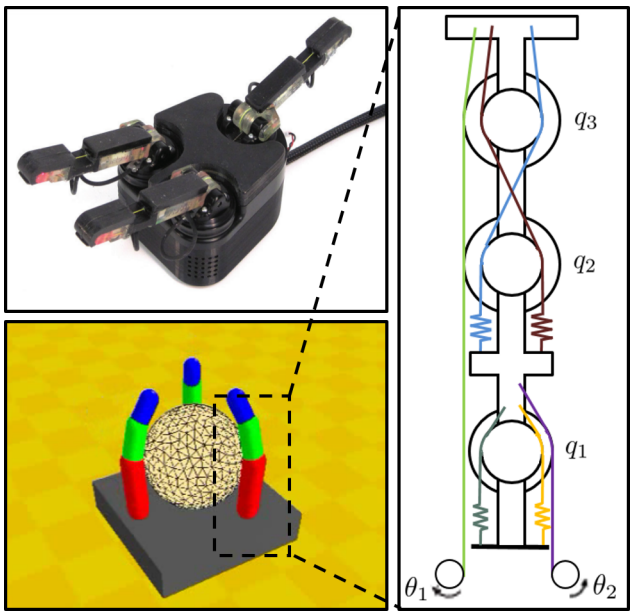

Figure 17. The iRobot-Harvard-Yale (iHY) Hand (left), the three fingered virtual UATD hand used in the simulation (middle), and the tendon routing of each finger (right.)

then be written by

$$\begin{bmatrix} M_r & 0 \\ 0 & M(q) \end{bmatrix} \begin{pmatrix} \ddot{x}_r \\ \ddot{q} \end{pmatrix} + \begin{bmatrix} B_r & 0 \\ 0 & C(q) \end{bmatrix} \begin{pmatrix} \dot{x}_r \\ \dot{q} \end{pmatrix} + \begin{bmatrix} K_r & -K_{rq} \\ -K_{rq}^T & K_q \end{bmatrix} \begin{pmatrix} x_r \\ q \end{pmatrix} = \begin{pmatrix} K_{vc} x_{hd} \\ f \end{pmatrix}$$

where $q := [x; \delta] \in \Re^6$, $x_r, x_{hd} \in$SE(2) are the maximal coordinates of the rigid box and the haptic device, $M_r = 0.001 I_{3\times3}$[kg] is the inertia of the rigid body, $K_{rq} := [K_{rq,x}; 0_{3\times3}] \in \Re^{3\times6}$ with $K_{rq,x} = 10^5 I_{3\times3}$ being the spring between the beam end and the rigid box, $K_r := K_{rq,x} + K_{vc} \in \Re^{3\times3}$ with $K_{vc} = 7500 I_{3\times3}$ being the virtual coupling spring, and B_r is the stabilizing damping for the virtual spring. We also set the rotation of x_{hd} to be zero, since Omega 3® is the device of E(3).

We then implement the virtual coupling according to (Lee et al. (2012)), that were derived to be applicable for the PMI while also enforcing (hybrid-time) two-port passivity of the virtual coupling. For instance, with no virtual coupling damping, the force feedback to the haptic device is given by:

$$f_{hd}(t) := -K_{vc}(x_{hd,k} - x_{r,k}), \quad t \in [t_k, t_{k+1})$$

which, even if containing $x_{hd,k}$ and $x_{r,k}$ instead of (continuous-time) $x_{hd}(t)$ and (acausal) $\hat{x}_{r,k}$, can still be passified by the device damping in the continuous-time domain and by the virtual damping B_r in the discrete-time domain. The device damping of our adopted Omega 3® device turns out to be fairly small. This then requires us to choose rather small force scaling factor $\alpha = 0.001$. This small α is in fact an inherent restriction imposed by the device itself (i.e., z-width (Colgate and Brown (1994))). See (Huang and Lee (2011); Lee et al. (2012)) for more details on the derivation and passivity of the virtual coupling for the PMI. Of course, we may choose larger (i.e., sharper) gain K_{vc} if we adopt less conservative techniques than the PD (proportional-derivative) type virtual coupling (e.g., passive set-position modulation Lee and Huang (2010)).

Profile of haptic feedback along the vertical z-direction of the haptic device during the interaction with the flexible beam is shown in Fig. 16, where the user haptically interacts with the (lossless/marginally-stable) flexible beam through the rigid box and virtual coupling, some formulated in generalized coordinates and some in maximal coordinates.

5.3. Under-Actuated Tendon-Driven Hand Grasping

The last example is the adaptive power-grip of virtual rigid ball by multi-fingered under-actuated tendon-driven (UATD) hand as shown in Fig. 17. For the hand, we emulate the configuration of the iRobot-Harvard-Yale (iHY) Hand (Odhner et al. (2014)). We yet model each finger to be constructed according to the design of (Ozawa et al. (2014)). For this case, it is then much more convenient to model each finger in generalized coordinates (i.e., joint angles), whereas the hand palm and the virtual ball in maximal coordinates in SE(3).

Each finger is of three-DOF, yet, with only two-DOF actuation via active tendons. See Fig. 17 for their tendon-routing (adopted from Ozawa et al. (2014)) with two active tendons (green and orange lines) and four passive tendons (other lines). The configuration of the UATD hand is then given by the nine joint angles $q \in \Re^9$, which are actuated by the six actuators (i.e., motors) with their angles denoted by $\theta \in \Re^6$. The total stiffness of the three fingers, stemming both from the active and passive tendons, can then be computed more conveniently in the joint angles q (i.e., generalized coordinates) s.t.,

$$K = J_a^T K_a J_a + J_p^T K_p J_p$$

where $K_a \in \Re^{6\times6}$, $K_p \in \Re^{12\times12}$ are the active and passive tendon stiffness, and $J_a \in \Re^{6\times9}$, $J_p \in \Re^{12\times9}$ are their

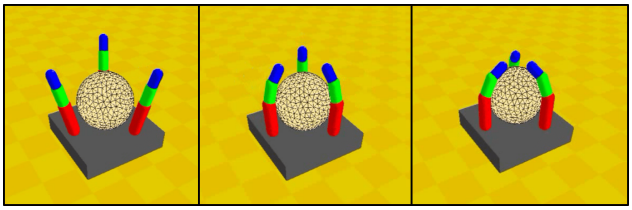

Figure 18. Snapshots of adaptive power-grasping of virtual rigid ball by the three-fingered UATD hand, with each finger having tendon-routing as depicted in Fig. 17, with the three fingers simultaneously controlled by one-DOF of the haptic device.

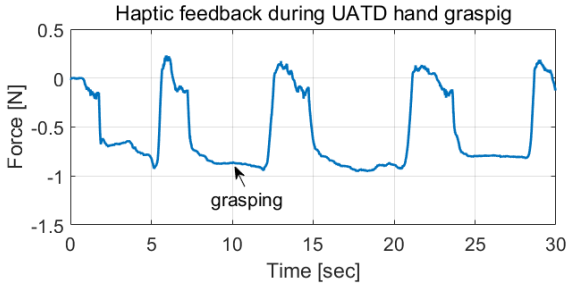

Figure 19. Haptic feedback of the one-DOF (i.e., z-directional) contact force of the adaptive power-grasping of the UATD hand in Fig. 18.

respective Jacobians. Here, K_a, K_p are typically assumed constant (i.e., linear tendon), whereas J_a, J_p are also constant, as they are defined by the pulley radii at each joint of the active and passive tendons, with $J_a q$ and $J_p q$ being their respective length change. The dynamics of the UATD hand can then be written w.r.t. the generalized coordinates q s.t.,

$$M(q)\ddot{q} + C(q,\dot{q})\dot{q} + Kq = f + f_c \tag{51}$$

similar to (4), where M, C are the inertia and Coriolis matrices, Kq is the total tendon compliance, f_c is the (external) grasping force, and f is the joint torque control input as given by

$$f = -J_a^T K_a R_a \theta =: -J_\theta \theta$$

where $R_a \in \Re^{6\times 6}$ is the matrix of the motor pulley radii (i.e., the tendon tension $K_a R_a \theta$ converted to the joint torque via J_a^T).

To control the adaptive under-actuated power-grip of this UATD hand, we use the Omega 3® haptic device as in Fig. 15 of Sec. 5.2. Here, we only use one-DOF of the haptic device (i.e., z-direction vertical motion) to command the power-grip. For this, we first map $z \in [z_{\min}, z_{\max}] \in \Re$ of the haptic device to the line interval $q^d \in \text{line}(q_1^d, q_2^d)$ of the UATD hand configuration s.t.,

$$q^d(z) := q_1^d + \frac{z - z_{\min}}{z_{\max} - z_{\min}}(q_2^d - q_1^d)$$

where q_1^d, q_2^d represent unfolded and folded configurations. Here, q_2^d is not necessarily required to form the shape of the object to grasp, since the UATD hand can adaptively grip objects with different shape via its tendon compliance and under-actuation. Then, using the quasi-static equation of (51), we can compute the following control input θ to attain $q^d(z)$ s.t.,

$$\theta = -(J_\theta^T J_\theta)^{-1} J_\theta^T K q^d(z)$$

Of course, the UATD hand in general cannot exactly follow this $q^d(z)$-command, since its dynamics (51) is under-actuated, thus, the contact force f_c can induce (unintended) deformation of the fingers. We provide this information to the user so that s/he can adjust the adaptive grasping in the form of the following haptic device force feedback:

$$f_z(z, z_{\text{proj}}(q)) := -k_{hd}(z - z_{\text{proj}}(q))$$

where $k_{hd} > 0$ is the feedback gain, z is the device current z-position, and $z_{\text{proj}}(q)$ the mapping of the UATD hand configuration q to the z-direction of the haptic device, s.t.,

$$z_{\text{proj}}(q) := z_{\min} + (z_{\max} - z_{\min})\frac{\|q - q_1^d\|}{\|q_2^d - q_1^d\|}.$$

Snapshots of this adaptive power-grip of the multi-fingered UATD hand are shown in Fig. 18 along with the contact force feedback in Fig. 19. For this, we use $K_a = 100 I_{6\times 6}$[N/m] and $K_p = 10 I_{12\times 12}$[N/m] with the mass of each link of the finger to be 0.001[kg]. From Fig. 18 and Fig. 19, we can then see that our PMI-based framework can stably simulate this power-gripping of UATD hand, through the PMI and the multi-point PMI-LCP formulated both for the fingers (i.e., in generalized coordinates: Sec. 4) and for the virtual ball and palm (i.e., in maximal coordinates: Sec. 3). Note also that the fingers are fairly light/stiff systems, which are difficult to stably simulate by using other techniques (e.g., SEI).

6. Summary and Future Research

In this paper, we develop a novel framework for haptic rendering and interactive simulation, that is based on the PMI (passive midpoint integrator), which is derived by directly enforcing passivity property in the discrete-time domain. We formulate this PMI-based framework for mechanical systems, both in maximal coordinates and generalized coordinates; and also devise PMI-LCP formulation to fully incorporate multi-point Coulomb friction contact modeling into these two coordinate settings. Thanks to its passivity property, our PMI-based framework allows us: 1) to tune the virtual objects freely by exploring wide-range of parameters in a modular manner; 2) to stably simulate very light/stiff objects (e.g., for transparency) even with variable/slow integration steps (e.g., due to intermittent multi-point contact); and 3) to emulate such marginally-stable/lossless/energy-conserving behaviors as harmonic oscillation of flexible objects or elastic contact between rigid objects. Further, our PMI-based framework provides implementation flexibility and convenience, by allowing for both the maximal and generalized coordinates, and also their combination, which are imperative to simulate some types of mechanical systems (e.g., multi-fingered UATD hand). These advantages are experimentally demonstrated in this paper by using the three illustrative examples: haptic operation of peg-in-hole task; haptic interaction with flexible beam; and adaptive power-grasping by multi-fingered UATD hand.

Some possible future research directions include: 1) extension of the PMI-based framework to large-scale deformable objects, including cut-and-joining and fluidic simulation; 2) combining the constraint-stabilizing potential and PMI-LCP formulation while respecting non-iterativeness and passivity of the PMI; 3) geometric properties of the coordinate transformation (36) and its application to other problems; 4) application of the PMI-based rendering for multi-user VR and haptic interaction over the Internet; and 5) development of open-source simulation platform based on our PMI-based simulation framework.

Acknowledgement

Research supported by the Global Frontier R&D Program on ⟨Human-Centered Interaction for Coexistence⟩ (NRF-2013M3A6A3079227), the Engineering Research Center Program for Soft Robotics (2016R1A5A1938472), and the Convergence Technology Development Program for Bionic Arm (2015M3C1B2052817) of the National Research Foundation (NRF) funded by the Ministry of Science, ICT & Future Planning (MSIP), Korea. The authors also would like to thank Mr. Hyunsoo Yang, Mr. ChangSu Ha and Mr. Juhyeok Kim for their help in preparing for the illustrative examples of Sec. 5.

References

Baraff, D. (1996), Linear-time dynamics using lagrange multipliers, *in* 'Proc. of the annual conf. on Computer graphics and interactive techniques', ACM, pp. 137–146.

Barbič, J. and James, D. L. (2008), 'Six-dof haptic rendering of contact between geometrically complex reduced deformable models', *IEEE Transactions on Haptics* **1**(1), 1–14.

Bathe, K.-J. (2007), 'Conserving energy and momentum in nonlinear dynamics: a simple implicit time integration scheme', *Computers & Structures* **85**, 437–445.

Bender, J., Müller, M., Otaduy, M. A. and Teschner, M. (2013), Position-based methods for the simulation of solid objects in computer graphics., *in* 'Eurographics (STARs)', pp. 1–22.

Brown, J. M. and Colgate, J. E. (1997), Passive implementation of multibody simulations for haptic display, *in* 'Proc. of ASME Int'l Mechanical Engineering Congress & Exposition', pp. 85–92.

Brown, J. M. and Colgate, J. E. (1998), Minimum mass for haptic display simulations, *in* 'ASME Dynamic Systems & Control Division', pp. 249–256.

Buerger, S. P. and Hogan, N. (2007), 'Complementary stability and loop shaping for improved human-robot interaction', *IEEE Transactions on Robotics* **23**(2), 232–244.

Bullet (2007), 'Bullet physics engine'.
URL: *http://bulletphysics.org/wordpress/*

CHAI-3D (2004), 'Computer haptics and active interface'.
URL: *http://www.chai3d.org/*

Chung, J. and Hulbert, G. M. (1993), 'A time integration algorithm for structural dynamics with improved numerical dissipation: the generalized-α method', *Journal of Applied Mechanics* **60**, 371–375.

Cline, M. B. and Pai, D. K. (2003), Post-stabilization for rigid body simulation with contact and constraints, *in* 'Proc. of IEEE Int'l Conf. on Robotics and Automation', Vol. 3, IEEE, pp. 3744–3751.

Colgate, J. E. and Brown, J. M. (1994), Factors affecting the z-width of a haptic display, *in* 'Proc. IEEE Int'l Conf. on Robotics & Automation', pp. 3205–3210.

Colgate, J. E. and Schenkel, G. (1997), 'Passivity of a class of sampled-data systems: application to haptic interfaces', *Journal of Robotic Systems* **14**(1), 37–47.

Colgate, J. E., Stanley, M. C. and Brown, J. M. (1995), Issues in the haptic display of tool use, *in* 'Proc. of IEEE/RSJ Int'l Conf. on Intelligent Robots & Systems', Vol. 3, pp. 140–145.

Cottle, R. W., Pang, J.-S. and Stone, R. E. (2009), *The linear complementarity problem*, Vol. 60, Siam.

Courtecuisse, H., Adagolodjo, Y., Delingette, H. and Duriez, C. (2015), Haptic rendering of hyperelastic models with friction, *in* 'Proc. of IEEE/RSJ Int'l Conf. on Intelligent Robots & Systems', pp. 591–596.

Delingette, H. (1998), 'Toward realistic soft-tissue modeling in medical simulation', *Proceedings of the IEEE* **86**(3), 512–523.

Drumwright, E. (2008), 'A fast and stable penalty method for rigid body simulation', *IEEE Transactions on Visualization & Computer Graphics* **14**(1), 240–231.

Duriez, C., Dubois, F., Kheddar, A. and Andriot, C. (2006), 'Realistic haptic rendering of interacting deformable objects in virtual environments', *IEEE Transactions on Visualization & Computer graphics* **12**(1), 36–47.

Fotoohi, M., Sirouspour, S. and Capson, D. (2007), 'Stability and performance analysis of centralized and distributed multi-rate control architectures for multi-user haptic interaction', *International Journal of Robotics Research* **26**(9), 977–994.

Garre, C., Hernández, F., Gracia, A. and Otaduy, M. A. (2011), Interactive simulation of a deformable hand for haptic rendering, *in* 'Proc. of World Haptics Conference', IEEE, pp. 239–244.

Garre, C. and Otaduy, M. A. (2010), 'Haptic rendering of objects with rigid and deformable parts', *Computers & Graphics* **34**(6), 689–697.

Hadap, S. (2006), Oriented strands - dynamics of stiff multi-body system, *in* 'Proc. of ACM SIGGRAPH/Eurographics Symposium on Computer Animation', pp. 91–100.

Hairer, E., Lubich, C. and Wanner, G. (2006), *Geometric numerical integration: structure-preserving algorithms for ordinary differential equations*, Vol. 31, Springer Science & Business Media.

Hasegawa, S. and Fujii, N. (2003), Real-time rigid body simulation based on volumetric penalty method, *in* 'Proc. of IEEE Haptics Symposium', pp. 326–332.

Horn, R. A. and Johnson, C. R. (2012), *Matrix analysis*, Cambridge university press.

Huang, K. and Lee, D. J. (2011), Hybrid virtual-proxy based control framework for passive bilateral teleoperation over the internet, *in* 'Proc. IEEE/RSJ Int'l Conf. on Intelligent Robots & Systems', pp. 149–156.

Huang, K. and Lee, D. J. (2013), 'Consensus-based peer-to-peer control architecture for multiuser haptic interaction over the internet', *IEEE Transactions on Robotics* **29**(2), 417–431.

Huynh, D. Q. (2009), 'Metrics for 3d rotations: Comparison and analysis', *Journal of Mathematical Imaging and Vision* **35**(2), 155–164.

Kim, M., Jang, I., Lee, Y., Lee, Y. and Lee, D. J. (2016), Wearable 3-dof cutaneous haptic device with integrated imu-based finger tracking, *in* 'Proc. of IEEE Int'l Conf. on Ubiquitous Robots and Ambient Intelligence', p. 649.

Kim, M., Kim, J., Lee, Y. and Lee, D. J. (2017), On the passivity of mechanical integrators in haptic rendering, *in* 'Proc. of IEEE Int'l Conf. on Robotics & Automation', pp. 446–452.

Kim, M. and Lee, D. J. (2017), 'Improving transparency of virtual coupling for haptic interaction with human force observer', *Robotica* **35**(2), 354–369.

Knoop, S., Vacek, S. and Dillmann, R. (2005), Modeling joint constraints for an articulated 3d human body model with artificial correspondences in icp, *in* 'IEEE-RAS Int'l Conf. on Humanoid Robots, 2005.', IEEE, pp. 74–79.

Kolesnikov, M. and Zefran, M. (2007), Energy-based 6-dof penetration depth computation for penalty-based haptic rendering algorithms, *in* 'Proc. of IEEE/RSJ Int'l Conf. on Intelligent Robots & Systems', pp. 2120–2125.

Krysl, P. (2005), 'Explicit momentum-conserving integrator for dynamics of rigid bodies approximating the midpoint lie algorithm', *International Journal for Numerical Methods in Engineering* **63**(15), 2171–2193.

Krysl, P. (2006), 'Direct time integration of rigid body motion with discrete-impulse midpoint approximation: explicit newmark algorithms', *Communications in Numerical Methods in Engineering* **22**(5), 441–451.

Kuhl, D. and Crisfield, M. A. (1999), 'Energy-conserving and decaying algorithms in non-linear structural dynamics', *International Journal of Numerical Methods in Engineering* **45**, 569–599.

Lee, D. J. (2009), Extension of colgate's passivity condition to variable-rate haptics, *in* 'Proc. of IEEE/RSJ Int'l Conf. on Intelligent Robots & Systems', pp. 1761–1766.

Lee, D. J. (2010), 'Passive decomposition and control of nonholonomic mechanical systems', *IEEE Transactions on Robotics* **26**(6), 978–992.

Lee, D. J. and Huang, K. (2008), On passive non-iterative varying-step numerical integration of mechanical systems for haptic rendering, *in* 'Proc. of ASME Dynamic Systems & Control Conference'.

Lee, D. J. and Huang, K. (2010), 'Passive-set-position-modulation framework for interactive robotic systems', *IEEE Transactions on Robotics* **26**(2), 354–369.

Lee, D. J., Kim, M. and Qiu, T. (2012), Passive haptic rendering and control of lagrangian virtual proxy, *in* 'Proc. of IEEE/RSJ Int'l Conf. on Intelligent Robots & Systems', pp. 64–69.

Lee, D. J. and Li, P. Y. (2005), 'Passive bilateral control and tool dynamics rendering for nonlinear mechanical teleoperators', *IEEE Transactions on Robotics* **21**(5), 936–951.

Lee, D. J. and Lui, K. Y. (2017), 'Passive configuration decomposition and passivity-based control of nonholonomic mechanical systems', *IEEE Transactions on Robotics* **2**(33), 281–297.

Lee, D. J. and Spong, M. W. (2006), 'Passive bilateral teleoperation with constant time delay', *IEEE Transactions on Robotics* **22**(2), 269–281.

Lloyd, J. E. (2005), Fast implementation of lemke's algorithm for rigid body contact simulation, *in* 'Proc. of the IEEE Int'l Conf. on Robotics and Automation', pp. 4538–4543.

Marsden, J. E. and West, M. (2001), 'Discrete mechanics and variational integrators', *Acta Numerica* pp. 357–514.

Müller, M., Heidelberger, B., Teschner, M. and Gross, M. (2005), 'Meshless deformations based on shape matching', *ACM Transactions on Graphics* **24**(3), 471–478.

Murray, R. M., Li, Z. and Sastry, S. S. (1993), *A mathematical introduction to robotic manipulation*, CRC, Boca Ranton, FL.

ODE (2001), 'Open dynamics engine'.
URL: *http://www.ode.org/*

Odhner, L. U., Jentoft, L. P., Claffee, M. R., Corson, N., Tenzer, Y., Ma, R. R., Buehler, M., Kohout, R., Howe, R. D. and Dollar, A. M. (2014), 'A compliant, underactuated hand for robust manipulation', *International Journal of Robotics Research* **33**(5), 736–752.

Ortega, M., Redon, S. and Coquillart, S. (2007), 'A six degree-of-freedom god-object method for haptic display of rigid bodies with surface properties', *IEEE Transactions on Visualization & Computer Graphics* **13**(3), 458–469.

Otaduy, M. A. and Lin, M. C. (2006), 'A modular haptic rendering algorithm for stable and transparent 6-dof manipulation', *IEEE Transactions on Robotics* **22**(4), 751–762.

Otaduy, M. A., Tamstorf, R., Steinemann, D. and Gross, M. (2009), Implicit contact handling for deformable objects, *in* 'Computer Graphics Forum', Vol. 28, Wiley Online Library, pp. 559–568.

Ozawa, R., Kobayashi, H. and Hashirii, K. (2014), 'Analysis, classification, and design of tendon-driven mechanisms', *IEEE Transactions on Robotics* **30**(2), 396–410.

Peterlik, I., Nouicer, M., Duriez, C., Cotin, S. and Kheddar, A. (2011), 'Constraint-based haptic rendering of multirate compliant mechanisms', *IEEE Transactions on Haptics* **4**(3), 175–187.

Prattichizzo, D., Chinello, F., Pacchierotti, C. and Malvezzi, M. (2013), 'Towards wearability in fingertip haptics: a 3-dof wearable device for cutaneous force feedback', *IEEE Transactions on Haptics* **6**(4), 506–513.

Rakhsha, R. and Constantinescu, D. (2014), Passive shared virtual environment for distributed haptic cooperation, *in* 'Proc. of Haptics Symposium', IEEE, pp. 221–226.

Rao, S. S. and Yap, F. F. (1995), *Mechanical vibrations*, Vol. 4, Addison-Wesley New York.

Siciliano, B. and Khatib, O. (2008), *Springer handbook of robotics*, Springer Science & Business Media.

Simo, J. C., Tarnow, N. and Wong, K. K. (1992), 'Exact energy-momentum conserving algorithms and symplectic schemes for nonlinear dynamics', *Computer Methods in Applied Mechanics & Engineering* **100**, 63–116.

Simo, J. C. and Wong, K. K. (1991), 'Unconditionally stable algorithms for rigid-body dynamics that exactly preserve energy and momemtum', *International Journal of Numerical Methods in Engineering* **31**(Jan.), 19–52.

Slotine, J.-J. E. and Li, W. (1987), 'On the adaptive control of robot manipulators', *International Journal of Robotics Research* **6**(3), 49–59.

Spong, M. W., Hutchinson, S. and Vidyasaga, M. (2006), *Robot modeling and control*, John Wiley & Sons, Hoboken, NJ.

Vidyasagar, M. (1993), *Analysis of nonlinear dynamic systems*, second edn, Prentice Hall.

VREP (2010), 'Virtual robot experimentation platform'.
URL: *http://www.coppeliarobotics.com/*

Weinstein, R., Teran, J. and Fedkiw, R. (2006), 'Dynamic simulation of articulated rigid bodies with contact and collision', *IEEE Transactions on Visualization & Computer Graphics* **12**(3), 365–374.

Zilles, C. B. and Salisbury, J. K. (1995), A constraint-based god-object method for haptic display, *in* 'Proc. of IEEE/RSJ Int'l Conf. on Intelligent Robots & Systems', pp. 146–151.